This is a preprint. The final publication is available at Springer via http://dx.doi.org/10.1007/s00410-013-0872-7

TiO_2 exsolution from garnet by open system precipitation: Evidence from crystallographic and shape preferred orientation of rutile inclusions

Alexander Proyer*[1], Gerlinde Habler[2], Rainer Abart[2], Richard Wirth[3], Kurt Krenn[1] and Georg Hoinkes[1]

[1] Institute of Earth Sciences, University of Graz, Universitaetsplatz 2/II, A-8010 Graz, AUSTRIA
*Corresponding author, e-mail: alexander.proyer@uni-graz.at
Tel.: 0043-316-380-5541; Fax: 0043-316-380-9865
[2] Department of Lithospheric Research, University of Vienna, Althanstrasse 14, A-1090 Vienna, Austria
[3] Geoforschungszentrum Potsdam, Am Telegrafenberg, D-14473 Potsdam, Germany

Abstract

We investigated rutile needles with a clear shape preferred orientation in garnet from (ultra-) high pressure metapelites from the Kimi Complex of the Greek Rhodope by electron microprobe, Electron Back Scatter Diffraction and TEM-techniques. A definite though complex crystallographic orientation relationship between the garnet host and rutile was identified in that Rt[001] is either parallel to Grt<111> or describes cones with opening angle 27.6° around Grt<111>. Each Rt[001] small circle representing a cone on the pole figure displays six maxima in the density plots. This evidence together with microchemical observations in TEM, when compared to various possible mechanisms of formation, corroborates a precipitate origin. A review of exchange vectors for Ti-substitution in garnet indicates that rutile formation from garnet cannot occur in a closed system. It requires that components are exchanged between the garnet interior and the rock matrix by solid state diffusion, a process we refer to as "open system precipitation" (OSP). The kinetically most feasible reaction of this type will dominate the overall process. The perhaps most efficient reaction involves internal oxidation of Fe^{2+} to Fe^{3+} and transfer from the dodecahedral to the octahedral site just vacated by Ti^{4+}: 6 $M^{2+}_3TiAl[AlSi_2]O_{12}$ + 6 $M^{2+}_{2,5}TiAlSi_3O_{12}$ = 10

$M^{2+}_{3.0}Al_{1.8}Fe_{0.2}Si_3O_{12} + M^{2+} + 2\ e^- + 12\ TiO_2$. OSP is likely to occur at conditions where the transition of natural systems to open system behaviour becomes apparent, as in the granulite and high-temperature eclogite facies.

Introduction

This paper intends to clarify the genesis of rutile needles in garnet that show a clear and very strict shape-preferred orientation (SPO) in 3-4 easily observable directions controlled by the lattice of the host garnet. The rutile SPO itself is a strong argument for a solid state precipitation[1] origin, an explanation which was either openly or tacitly adopted by many researchers reporting similar observations from eclogite and garnet pyroxenite xenoliths in kimberlites (McGetchin and Silver, 1970; Griffin et al., 1971; Dawson, 1980, p. 152; Haggerty and Sautter, 1990; Fung and Haggerty, 1995; Wang et al., 1999, Roden et al. 2006), from upper amphibolite to granulite facies rocks (Griffin 1971, Vrana 1989, Whitney, 1992; Snoyenbos et al. 1995, O'Brien 1999, Liati et al., 2002, Parker et al., 2010, Kawasaki et al, 2011; Ague and Eckert, 2012) or plutons (Enea, 2008), or more recently from garnet peridotites and other high to ultrahigh pressure (UHP) rocks (Zhang and Liou 1998, Song et al., 2004, Bakun-Czubarow, 2004, Ye et al. 2000, Zhang et al. 2003). This was done in spite of the fact that a crystallographic preferred orientation (CPO) relationship between rutile needles and the garnet host was not established and even questionable as rutile needles show oblique extinction over a range of extinction angles rather than straight extinction. Another

[1] Following the usage of terminology in materials science and mineralogical literature, "precipitates" are daughter phases with a crystal structure different from the host phase, while "exsolutions" have the same or a very similar crystal structure as the host (Gottstein, 2001). For the process itself the words precipitation, exsolution or unmixing are used interchangeably.

problem with this interpretation is the fact that TiO_2 cannot exsolve stoichiometrically from garnet. This problem exists even in the cases of co-precipitation with other phases like ortho- and clinopyroxenes or even apatite (Ye et al. 2000). Efforts to explain TiO_2 precipitates in a closed system failed (Zhang et al. 2003). More challenges came up with the work of Perchuk (2008), who interpreted oriented lamellae of rutile and mica in garnets of diamond-bearing gneisses from Erzgebirge as reaction products between garnet and liquid inclusions and Hwang et al. (2007a), who investigated inclusions of rutile needles in garnets from UHP eclogites extensively by means of TEM and concluded that there was no clear crystallographic relationship between rutile and garnet. As the rutile formation could not be explained in terms of exsolution in a closed system, Hwang et al (2007a) discarded this genetic model and proposed several alternatives including fluid-assisted precipitation in microcleavages. Moreover, Harlov (2005) observed oriented inclusions of monazite growing in a hydrothermally altered rim of fluor-apatite, demonstrating that fluid-induced replacement processes may in some instances also create inclusions with a SPO relationship to the host. As the geological interpretation of a rock may differ significantly, depending on the true genesis of rutile needles or other inclusions with SPO in high-grade garnets, further investigation of this phenomenon was required. EBSD is a method of choice because it allows to obtain significantly larger datasets of crystallographic orientation measurements from larger sample areas than TEM analysis (Feinberg et al., 2004; Zhang et al., 2011). On the other hand, TEM can reveal dislocations, nanotubes and other possible intragranular pathways for fluid molecules that might have been effective during solid inclusion formation. Moreover, structural coherency across phase boundaries and other nanoscale phenomena relevant for the genetic interpretation may be recognized by TEM investigations (e.g. Hwang et al., 2007a).

A considerable number of scenarios of origin other than (1) solid state precipitation can be envisioned for rutile needle formation, like (2) recrystallization of primary inclusions during

high-temperature annealing, with the interface geometry controlled by the garnet structure (Whitney et al., 2004), (3) overgrowth of pre-existing rutile with SPO by garnet (Force et al., 1996), (4) inclusions with SPO formed during rapid growth of the host in graphitic rocks (Burton et al,, 1986), (5) coeval growth of garnet and rutile that attaches at the garnet's growth surfaces in an epitaxially controlled way (Wang et al., 1999), (6) crystallographically oriented fluid-alteration (etch-channels) of garnet with Ti introduced into the crystal and deposited as rutile needles in the channels, (7) formation of microcleavage followed by precipitation of foreign material and healing (Hwang et al. 2001, 2007a, b), (8) dissolution-precipitation, i.e. volume-replacement of garnet from the rims toward the interior and reprecipitation of garnet material with slightly different composition and minor components in the precursor garnet, mainly Ti, either carried away or precipitated in situ at the replacement front, and (9) interaction of garnet with melt (Perchuk, 2008).

Only the first two mechanisms are classically considered to operate in a closed mineral system, i.e. within a (solid solution) crystal without material exchange across the grain boundary. The remaining seven involve reactions with other phases or processes at the growth front of the crystal. Proyer et al. (2011) pointed out that even during precipitation a crystal is more or less open to the matrix and can exchange ions and other species. The degree of openness depends on the type of species and the available transport pathways. In "open system precipitation" sensu stricto (by "system" we mean the solid solution crystal, not the rock), transport is mainly accomplished by volume diffusion through the host crystal. OSP sensu lato occurs when dislocations, nanotubes or subgrain boundaries become additionally relevant pathways for material transport. During OSP the original grain boundary remains more or less in place, so mechanisms like dissolution-precipitation or others would not be included in the definition. The original definition by Proyer et al. (2009) included the criterion that precipitation is accomplished only due to diffusional material exchange with the rock

matrix. OSP behaviour is not really limited to such cases, but it is only in such cases that open-system behaviour is an obvious requirement.

The purpose of this paper is to present detailed EBSD and TEM work on a sample that contains almost exclusively rutile inclusions with shape preferred orientation in garnet in order to demonstrate that the main criterion for a precipitate origin – a clear SPO accompanied by CPO – is actually fulfilled. Due to the non-stoichiometry of rutile exsolution from garnet some sort of open-system behaviour must have occurred. The characteristic criteria for each of the nine envisioned mechanisms of formation will be evaluated against the observations in the discussion part. We will demonstrate that open system precipitation as defined above is the most likely mechanism of formation.

(

SAMPLE DESCRIPTION

The type of sample material described here comes from the Kimi Complex of the Greek Rhodope massif for which a complex tectono-metamorphic evolution including an early stage of ultrahigh-pressure metamorphism (UHPM) has been described in a series of recent papers (Ricou et al., 1998; Liati et al., 2005, Bauer et al., 2007, Krenn et al., 2010; Schmidt et al., 2010; Nagel et al., 2011). Several garnets from metapelitic gneisses of the Kimi Complex were found to contain microdiamonds and were consequently interpreted to have undergone an ultrahigh-pressure stage in their metamorphic evolution (Mposkos and Kostopoulos, 2001; Perraki et al. 2006; Krenn et al., 2010, Schmidt et al., 2010). Abundant, very fine grained rutile needles showing shape preferred orientation are also typical for garnets from the diamond-bearing gneisses. Rutiles can be associated with small but variable amounts of

quartz, apatite, kyanite, zircon or biotite of similar grain size, distribution and idiomorphic, often elongate habitus pointing to a common origin.

Sample 2R5 is taken from a garnet-kyanite-bearing micaschist from the Xanthi area. It contains centimetre-sized subidiomorphic garnets embedded in a matrix of kyanite, muscovite, biotite, quartz, and plagioclase. Accessory minerals are rutile, apatite, zircon and monazite. In this paper we describe one of many single large garnets (about 30 mm in diameter) from sample 2R5 with an extremely poikilitic, diamond-bearing garnet core surrounded by a clear 2-4 mm thick rim in which abundant, regularly spaced and crystallographically oriented rutile predominates the inclusion population (97% in number and >99% in volume; see Table 1 and description below). Less conspicuous platelets and more isometric shaped rutile inclusion of micron to submicron scale have also been observed amongst the needles in the rim (Fig 3a, b). The rutiles are evenly distributed throughout the rutile-bearing domain and detailed observation reveals that the needles show shape preferred orientation in up to six directions. Three to four of them are readily identified, whereas the remaining directions are either less common or more difficult to detect due to almost vertical plunge of the needles. Within each group the long axes of the needles are strictly aligned. The constant angular relations among the alignment directions suggest a crystallographic control (Fig 3b). The very outer margin of the garnet (a few 10s of microns) is completely free of inclusions. A detailed composition profile of this garnet including the minor elements Na, P, Ti, Cr, Y and Zr is drawn in Fig. 1c The profile shows a rise of both Mn and Y after a fall between the core and rim of the garnet, which most likely indicates a period of resorption. Ti and P rise in the rim to about 0.045 and 0.015 wt% of the oxides or 0.002 and 0.003 a.p.f.u. respectively. Na correlates with Y in the garnet core but shows no clear correlation with Y, Ti or P in the rim. The major element profile indicates a strong rise of the Mg content and a concomitant drop in Fe-content in the rutile-bearing clear rim (Fig 1c). The TiO_2 content of a re-integrated garnet compositions (from image analysis) would be ca. 0.25 wt%. Biotite varies

considerably in grain size and large grains remote from garnet preserve compositional zoning with Mg- enriched cores. The variation in muscovite grain size is less conspicuous, but compositional zoning is more prominent, with Si- and Mg- enriched cores. Many of the plagioclase grain display three compositional zones: an albite-rich core, an intermediate zone and an outer margin with the highest anorthite content. *PT*-conditions were calculated for the oldest preserved mineral assemblage (cores of plagioclase and micas and outer margin of the needle-bearing garnet zone), using classical geothermobarometers (mainly garnet-biotite thermometer and GASP) with the software PET (Dachs 1998, 2004) and the average-*PT* mode of THERMOCALC (Powell and Holland, 1994) and the results are 620-660°C and 11-16 kbar (PET) and 850 ± 50°C and 14.5 ± 1.8 kbar (TC) respectively. The discrepancy is mainly due to the fact that the garnet-biotite temperatures used in the first approach are highly prone to resetting during cooling, and the average-PT result is considered to be more robust and reliable. The optimal result in average-*PT* is obtained by using the most Mg-rich garnet compositions from the needle-zone together with Ca-rich plagioclase and less phengitic muscovite, even though the latter two factors do not shift the *P-T* result significantly. Even though there is considerable uncertainty about the actual *P-T* path of this rock, the Mg-rich rim with its increased levels of P and Ti most likely formed during a granulite facies stage along the exhumation path rather than at UHP conditions. The Na-content of garnet does not correlate with Ti or P in the rim, as in the high-pressure substitution $NaTiCa_{-1}Al_{-1}$ (Ringwood and Major, 1971; Sobolev and Lavrent'yev, 1971) and $NaPCa_{-1}Si_{-1}$ (Brunet et al., 2006) but with Y in the garnet core, a substitution which does not require high pressures (Enami et al., 1995). There are no conspicuous microstructural indicators for decompression melting in the rock, and plagioclase zoning is also inconsistent with the (former) presence of melt unless the melt was almost completely extracted. The latter scenario would explain all the observations, including plagioclase zoning (caused by batch melting) and the high *P-T* values obtained from average-*PT*.

Inclusion details

A series of equal area rectangles within the clear rim of a single garnet grain (ca. 4 cm in diameter) in sample 2R5 were selected to identify and count the small inclusions using BSE imaging and EDX analysis. On our 2D-sections all inclusions listed in Table 1 are smaller than 10 µm and ~98% of these inclusions are smaller than 2 µm, with the only exception of characteristic larger grains interpreted as primary rutile inclusions. Other large inclusions occasionally occurring in the studied domains are described separately (see footnotes to the table). Phase identification was mainly based on EDX data, although compositions could only be determined semi-quantitatively due to the small grain size of the inclusions. Kyanite was identified as the Al_2SiO_5 polymorph using Raman spectroscopy.

Within the 4 mm thick, clear rim of garnet there is a marked predominance of rutile inclusions (Table1). In BSE images, the rutile crystal sections are mostly isometric and rarely acicular with diameters of 1-2 µm or less (Fig. 5). Only rarely up to 10 µm sized grains are observed. Quartz and kyanite are commonly smaller than 2 µm, and only in a few instances quartz reaches several micrometers in diameter. Note that rutile, quartz and kyanite are occasionally also found in contact (polymineralic inclusions). Carbonate phases (dolomite or ankerite) are rarely smaller than 2 µm. They rather lie in the 5-10 µm size range and then are often associated with voids indicating a possible fluid inclusion origin. Other µm-sized inclusions are rare: In some places tiny zircons are associated with rutile needles, whereas another about 10 µm sized zircon grain is interpreted to be primary. Apatite of 1 µm size was found in one location only.

ANALYTICAL METHODS

Electron Backscatter Diffraction (EBSD):

The crystallographic orientation relations between 213 rutile-grains and the garnet host grain were determined by Electron Back Scatter Diffraction (EBSD) spot measurements using a FEI™ Quanta 3D FEG instrument at the Department of Lithospheric Research (University of Vienna, Austria). This instrument is equipped with a NG Schottky electron field-emitter and an EDAX™ Digiview IV EBSD camera. The rock sample was prepared as polished thin section by mechanical and final chemo-mechanical polishing with colloidal silica suspension (pH 9.2-10) as polishing medium on a rotary polisher. Very thin carbon coating of the sample surface has been performed using a single carbon thread at vacuum conditions of $<1.10^{-5}$ mbar during evaporation in order to establish conductivity. Analyses have been performed at a working distance of 10 mm and a beam incidence angle of 20° with the sample surface. Electron beam conditions were at 20 kV accelerating voltage and 4 nA beam current in analytic mode using a 1 mm SEM aperture. A 2x2 binning of the EBSD camera-resolution has been applied as well as Hough settings of 2° theta step size, a binned pattern size of 120 pixels and a 9x9 convolution mask for indexing 6-12 Hough peaks. The OIM™ Data Collection and Analysis software packages have been used for data processing.

TEM

Site specific and spatially oriented TEM foils (10 x 6 x 0.1 µm sized) were prepared using Focused Ion Beam (FIB) technique. FIB preparation was done on a FEI™ Quanta 3D FEG Dual Beam™ instrument at the Department of Lithospheric Research, University of Vienna, Austria. This instrument is equipped with a field emission Ga-source, Pt and C gas injection systems and an Omniprobe™ 100.7 micromanipulator for in situ lift out of the thinned foils. During foil preparation ion beam currents of 50 -1 nA have been used for rough cuts and 500 – 30 pA for foil thinning at successively smaller beam currents. The accelerating voltage was at 30 kV throughout the sputtering and gas deposition procedure. Pt was used for mechanical stabilization and mounting of the foils to a Cu grid.

We used analytical and energy-filtered high-resolution transmission electron microscopy (ATEM, HRTEM) on a Tecnai F20 X-Twin TEM at the GFZ Potsdam operated at 200 kV with a field emission gun (FEG) electron source. The TEM is equipped with a post-column Gatan imaging filter (GIF Tridiem). All of the TEM images presented are energy-filtered images, where a 10 eV window was applied to the zero loss peak. The Gatan DigitalMicrograph software was used to analyse the transmission electron micrographs. ATEM was performed with an EDAX X-ray analyser equipped with an ultrathin window. The X-ray intensities were measured in the scanning transmission mode (STEM) scanning the electron beam in a preselected window thus avoiding mass loss during data acquisition.

RUTILE-GARNET ORIENTATION RELATIONS

Shape preferred orientation of rutile

Transmitted light microscopy showed four common directions of rutile needle shape preferred orientation, which are orthogonal to each other as measured using a universal stage. Two additional sets of needle SPO are much less abundant. They also display an orthogonal spatial relationship to each other but the angular relationship to the dominant four sets could not be measured as they were out of range for the universal stage. Almost none of the needles show parallel extinction using crossed polarized light. The angle of extinction varies considerably within each set, even though a number of parallel needles in close vicinity seem to have a similar angle of extinction.

Crystallographic preferred orientation of rutile

From Electron Back Scatter Diffraction analyses the garnet host is identified as a single crystal (Fig. 4a, b). Spot analyses of 213 rutile needles enclosed in the outer zone of a single garnet crystal of sample 2R5 reveal complex, though systematic orientation relations between

the lattices of the rutile needles and the garnet host (Fig. 4). Only a small fraction of the rutiles has the c-axes oriented parallel to Grt<111>. The majority of the rutile needles show a more complex crystallographic orientation relation to the garnet host, as Rt[001] directions describe cones around Grt<111> (Fig 4a, c). The angle enclosed by Grt<111> and the Rt[001] directions yielded an average of 27.6° (ranging at 26 – 29 °). Density plots show that the rutile c-axis orientations are not evenly distributed along the small circles around the Grt <111> directions. They rather cluster at 6 positions along every small circle, which may be grouped into 3 double maxima (Fig 4a). The c-axis orientation maxima have a defined orientation relation with the garnet lattice, as they cluster around Grt <110> at an angular misorientation of 10-13°. Therefore a special orientation of the rutile lattice exists which is repeated by the Grt{101} mirror planes and by the Grt<111> three fold axes.

Furthermore, the rutiles with Rt[001] describing a cone around Grt<111> have an entirely fixed crystallographic orientation with respect to the garnet lattice. Poles of Rt(101) planes corresponding to one Rt[001] cone form three small circles at different misorientation angle around the respective Grt[111] direction (Fig. 4d). Two of the four Rt(101) poles lie at the same small circle, thus having the same angular misorientation with respect to Grt[111]. These poles form the intermediate small circle. The other two Rt(101) poles lie within a plane defined by Rt[001] and Grt[111] and form an inner and outer small circle around Grt[111]. The Rt a-axes corresponding to one Rt[001] cone form two small circles around the respective Grt[111] with one a-axis lying in the plane comprising Rt[001] and Grt [111] (Fig. 4f). Consistently, all Rt<110> directions of one Rt[001] cone form one small circle around the respective Grt[111] direction (Fig 4e). This indicates that the rutiles with their Rt[001] directions on a small circle around Grt <111> cannot rotate freely around their c-axes, but have one a-axis oriented in the plane comprising Grt[111] and Rt[001] as well as one tangential to the cone. Furthermore, a set of Rt[100] directions corresponding to one Rt c-axes cone around one Grt[111] direction is oriented within a plane, which also comprises two Grt

[110] directions. Still correlated Grt [110] and Rt [100] do not coincide, but Rt [100] directions cluster at maxima with 15° misorientation with respect to Grt [110]. Although rather complex, these orientation relations suggest a strict topotactic relation between the rutile needles and the garnet host.

Rutile-garnet interface structure

Three representative FIB foils were prepared for TEM analysis. Figures 5a-j shows transmitted light photographs, and SE images of the thin section and the cut foils as well as the Rt [001] orientation of each selected rutile grain. R7 is a cross section and R164 is a longitudinal section of rutile needles, which have their c-axis on a Rt [001] maximum of a cone around Grt<111> (Fig. 5j), whereas foil R132 contains two isometric rutile grains: grain 1 was measured by EBSD and its c-axis plots off a Rt[001] cone, grain 2 was completely surrounded by garnet (no EBSD data available) and is definitely not acicular (cf. Fig. 5g). Bright field images (Figs 6a-c) show that grain R132-2 is idiomorphic, with smooth grain boundaries, except one irregularly embayed section which goes along with strong strain contrast: The HRTEM-Image (Fig. 6d) shows the ruggedness of the garnet-rutile interface. The diffraction pattern (Fig. 6d – inset) reveals substantial misfit between the lattices of garnet and rutile. Grain 1 is also idiomorphic, with minor irregularities along one boundary and accompanying minor strain contrast (Fig. 6e). No common low-indexed zone axis was found for R132-1 or R132-2 with garnet within the accessible tilting range (α-tilt 30°, β-tilt 20°)

Rutile grain R164 has an elongate idiomorphic grain shape with an additional phase (bright) at the irregularly shaped tip (Fig. 7a). EDX analyses indicate that this additional phase – an oxide – contains Al, Zn, Fe and Mg (Fig. 7b, Table 2). The diffraction pattern (Fig. 7c) could be indexed as that of Zn-rich spinel, based on d-spacings given in Andreozzi et al. (2001).

Figure 8a shows thickness and strain contrasts in R164 in more detail, and a close-up of the corner (Fig. 8b) demonstrates that the diffraction contrast extends across the fine bright boundary line. Hence, this line cannot be an amorphous boundary layer.

High-resolution images of the corner (Fig 8c) and of the flat tip (Fig. 8d) show a stepped and flat grain boundary respectively and again document the lack of an amorphous boundary layer.

Also shown in Fig. 8d are indexed lattice planes of garnet and rutile. The common zone axes are $[1\text{-}2\text{-}1]_{ga}$ and $[1\text{-}13]_{ru}$. The garnet-rutile interface corresponds to {110} grt and $\{3\text{-}3\text{-}2\}_{ru}$, and the two corresponding lattice planes perpendicular to the grain boundary are $(222)_{grt}$ and $(110)_{ru}$. From the diffraction pattern (Fig. 8e) substantial misfit is identified across the phase boundary even in this configuration. A mean a_0 value of 11.533 Å of garnet was calculated from the three imaging vectors in the garnet diffraction pattern after calibration of the camera constant from the rutile diffraction pattern using the (110) reflection. This results in a d-value for the garnet (222) of 3.3293 Å, which, compared to the d-value of (110) rutile of 3.2477 Å shows a difference of 0.0816 Å (ca. 2.5%). The angular misorientation is 1.4°.

In summary, the longest segments of the garnet-rutile interface are those with the least strain contrast; the long boundary at the tip has a stronger strain contrast which corresponds to the $(110)_{ru} - (222)_{grt}$ misfit just documented, and the two short boundary planes at the tip have the highest strain contrast and a stepped grain boundary.

The cross section of the rutile needle R7 also shows an idiomorphic grain shape (Fig. 9a). A bright zone along the lower left tip which is not crossed by the diffraction contrast indicates that an amorphous zone is present. This feature was observed already prior to any serious electron bombardment during TEM analysis, and is therefore definitely not a product of radiation damage. EDX analyses of this zone and adjacent garnet are shown for comparison in Table 2. Disregarding the influence of Ti from rutile (long range secondary fluorescence), the amorphous zone has significantly higher Si and Al, and lower Ca, Mg and Fe contents than

the garnet matrix. A composition profile across the boundary (Fig. 9b) shows a very minor but significant change in Si, Ca and Fe within the amorphous zone, with Si enrichment towards the rutile side and Ca and Fe enrichment towards the garnet side. Rutile is almost pure Ti-oxide, with minor amounts of Fe (Table 2). High-resolution images from the other phase boundaries demonstrate direct lattice contact, i.e. the absence of an amorphous zone (Fig. 9c). Even though common zone axes can be derived from the diffraction pattern (Fig. 9e) – the rutile c-axis $[001]_{ru}$ // $[-719]_{grt}$ –, the high index of the garnet axis demonstrates that the lattice fit is very poor. The multiplication of reflections in $[110]_{ru}$ (Fig. 9e) and the HRTEM images of rutile (Fig. 9d) indicate a platelet-type superstructure of poorly-ordered and well-ordered domains parallel to the rutile c-axis, a phenomenon of non-stoichiometric rutile (condensation/ordering of oxygen vacancies, mostly compensated by Ti^{3+} or Fe^{3+}, into platelets: Bursill et al., 1984; Banfield and Veblen, 1991).

DISCUSSION

Shape preferred orientation (SPO)

In their detailed TEM-investigation of inclusion-host relationships between several rutile needles and their garnet host from a UHP-eclogite, Hwang et al. (2007a) found that the needle long axes are strictly aligned parallel to the Grt<111> direction and that the rutiles are bounded by Grt(110) planes. They could, however, not find any rational orientation relation between the lattices of the rutiles and the garnet host.

Guinel and Norton (2006) investigated star garnets from Emerald Creek, Idaho, U.S.A. They do not mention angles of extinction but concluded from crystallographic arguments and TEM data that extremely fine grained rutile needles causing asterism in four rayed star garnets have two sets of rutile needles aligned along the Grt<111> directions. An additional set of rutile needles aligned along a <011> direction is developed in six-rayed star garnets. Preliminary U-stage measurements on sample 2R5 indicate that the dominant sets of rutile needles are

aligned parallel to Grt<111> and the subordinate sets possibly parallel to Grt<100>. However, the latter remains a crude guess because the shape orientation of these rutiles was out of the limited range required for precise measurements.

Zhang et al. (2003) already state that "most rutile rods are oriented along Grt<111> and the rods connect Al^{VI} sites in the garnet structure". This is also the site where Ti^{4+} resides in garnet, so such a growth direction may represent the fastest direction to connect TiO_6-coordination polyhedra to form rutile and could explain the morphological growth direction of the rutile needles. Grt<110> and Grt<100> are both directions in which octahedral sites alternate with dodecahedral sites, which is kinetically less favourable for lattice reconstruction.

Crystallographic preferred orientation (CPO)

Hwang et al. (2007a) claimed that "a solid state precipitation process always involves epitaxial nucleation for a lower activation energy and minimization of the interfacial strain", and asserted that a strict crystallographic orientation relation has to be expected between the newly formed phase and the host crystal. As they found no specific CPO between acicular rutile and the garnet host, they discarded precipitation as a possible mechanism of formation. Guinel and Norton (2006) did find crystallographic relationships, e.g. their TEM data on one rutile needle showed that it is elongated parallel to it's a-axis [010], which coincides with the [011] direction of the garnet host. Furthermore they observed thecrystallographic orientation relationships $[011]_g//[0\text{-}10]_r$, $(02\text{-}2)_g//(100)_r$, $(\text{-}400)_g//(001)_r$ for one set of rutile needles in a star garnet from Idaho which they investigated in detail by TEM. Based on this evidence, they proposed a precipitate origin of the rutile needles.

In our new dataset the crystallographic orientation relation described by Guinel and Norton (2006) is developed only to a minor extent. Only a few rutile grains in the new dataset show Rt<010> // Grt<110>, but have their Rt[001] oriented parallel to Grt<111>, which is the

subordinate lattice orientation relation of garnet and rutileThis crystallographic orientation relation described by Guinel and Norton (2006) is therefore confirmed by our data, but does not seem to represent the most favorable lattice orientation of rutile needles with respect to the garnet host in our sample. The second orientation relation of Grt(400) // Rt(001) described by Guinel and Norton (2006) is not reflected by our sample.

Instead, our EBSD study demonstrates that there is a definite, though complex crystallographic orientation relation between the garnet host and the rutile inclusions in sample 2R5. The majority of the rutile needles show preferred crystallographic orientations controlled by the garnet lattice. However, the EBSD data (Fig. 4) do not document only one single preferred orientation relation. The rutile c-axis may either coincide with the Grt<111> direction or –more frequently- describe a cone around those. The latter grains seem to take a crystallographic orientation with Rt[001] at an angular misorientation of c 27.6 ° with respect to Grt <111>. Furthermore Rt grains with the c-axis along a cone around Grt <111> cannot rotate freely around the c-axis, but have a fixed orientation with respect to the garnet lattice. Still some rutile orientations seem to scatter unsystematically. This complex relationship is reflected in the TEM-results – both our own (small up to considerable misfit at the grain contacts) and in those of Hwang et al. (2007a), who state that "except for the gross alignment between Grt<111> and Rt{101} poles, there are no specific crystallographic orientation relationships...". The latter authors were cautious to see a (reasonable) crystallographic relationship in their investigated samples from Sulu and the Bohemian Massif because they did find a good relationship in other samples from Kockchetav (shown in their appendix), with $[001]_{rt}$ //$[001]_{grt}$ and $\{100\}_{rt}$ //$\{110\}_{grt}$ or $<101>_{rt}$//$<111>_{grt}$ and $\{-101\}_{rt}$ //$\{1\text{-}10\}_{grt}$.

At any rate there seem to be differences in crystallographic orientation relationships between garnet and rutile, which is consistent with earlier observations. Griffin et al. (1971) showed that rutile needles with shape preferred orientation from some areas have their c-axes parallel to the needle long axis (straight extinction), whereas others do not (oblique extinction). This

points to a change in crystallographic orientation relations between garnet and rutile depending on factors like *P-T* conditions of formation (the exhumation history). The complex orientation relations between the rutile needles and the garnet host could only be identified in our study because of the relatively large number of EBSD point analyses. Although Hwang et al. (2007a) could not recognise this complex regularity from the seven investigated rutile grains, still 5 of these data points show a position of the rutile c-axis along a cone around Grt <111> as described here.

An assessment of the possible mechanisms of formation

In the following we describe the main characteristics of each of the nine processes outlined in the introduction and compare them with those of sample 2R5 in order to determine the most likely or dominant mechanism of formation for the oriented rutile needles in this sample.

(1) Precipitation in the solid state occurs when a solid solution component (or theoretical endmember) included at elevated P-T conditions becomes sufficiently unstable to cause uphill diffusion and nucleation of a new phase into which the unstable component can concentrate. Because of the extremely small size of the nucleus, interface energy is the dominant factor controlling its stability. If the crystal structure of the host mineral is relatively undisturbed (low number of dislocations, subgrain boundaries etc.), most precipitates will result from homogenous nucleation. In this case interface energy is determined by the relative crystallographic orientation of nucleus and host and can be minimized to the degree that structural similarities exist. As the nucleus grows to nanometre size and beyond, the elastic strain caused by the growing precipitate becomes the dominant energy term and structural coherency across the interface is gradually lost even though a general orientation relationship will continue to exist. Typical features for precipitates in the nano- to micrometre range therefore are: A general orientation relationship (SPO and CPO) while interfaces

range from semi-coherent to incoherent, a rather regular spacing between individual precipitate grains and precipitate-free zones (PFZ) near fast diffusion pathways (subgrain, grain and phase boundaries, dislocations, nanotubes etc.). Depending on the cooling history there may be several generations of precipitates with distinctly different average grain size. The most common types of precipitates have either platelet or needle shapes, as reasonably good lattice coherence exists in two or only one dimension respectively. (e.g. Doherty, 1983; Dent Glasser et al., 1962). The entire set of features described in the petrography, EBSD and TEM sections is consistent with a precipitate origin and there is more positive evidence from other sources: Guinel and Norton (2006) have confirmend a CPO relationship between garnet and rutile needles in star garnets from Idaho, and Ague and Eckert (2012) present extensive microprobe data (composition maps and profiles across the same type of oriented rutile needle inclusions in garnet) that demonstrate depletion halos for Ti and Cr around acicular rutile, which is a strong argument for a precipitation origin. The latter authors also describe a second, subordinate type of minute rutile inclusions (mainly platelets, often twinned) that might correspond to our own small subset of unoriented rutile inclusions that could correspond to situations of heterogeneous nucleation.

(2) As a result of EBSD work on inclusions in garnets from metapelitic rocks of different metamorphic grade, Whitney et al. (2004) noted that "quartz, plagioclase and other inclusions in garnet exhibit incipient facets in upper staurolite and kyanite facies rocks and are well faceted in sillimanite zone and higher grade rocks. The orientation of facets corresponds to the crystallographic orientation of host garnet." It is not clear to what extent rutile can be affected by such an annealing phenomenon. We have observed faceted primary quartz inclusions in garnets from other samples of the area, but primary, stubby rutile inclusions seem to be unaffected by annealing. The regular

distribution of the rutile needles contradicts a primary inclusion origin, but their faceting may well be influenced to some extent by annealing.

(3) Overgrowth of a pre-existing oriented network of rutile needles is a valid mechanism and depends on the presence of a suitable precursor phase that decomposes to form such networks. Both biotite and ilmenite are known to decompose to two-dimensional networks of rutile, and the product is loosely called sagenite (Armbruster, 1981, Shau et al., 1991). The only three-dimensional rutile network known forms after ilmenite which itself has exsolved from Ti-bearing magnetite as lamellae oriented in three dimensions (Force et al., 1996). We consider it highly unlikely that all the diamond-bearing garnet cores in sample 2R5 were once encrusted by titanoan magnetite.

(4) (Burton et al, 1986) describe sector-zoned garnets with abundant quartz inclusions that show nice elongation and shape preferred orientation perpendicular to the growth faces. This feature seems to be typical for the growth of porphyroblasts in graphite-bearing schist and is known also for staurolite, kyanite or andalusite (chiastolite). In such a case the SPO does not go along with a CPO – the orientation of the quartz c-axes with regard to the garnet crystal is random. The SPO differs between growth sectors but is the same within each sector. Both observations are inconsistent with our evidence for rutile in 2R5.

(5) Wang et al., (1999) in their investigation of oriented needle- and blade-shaped oxide inclusion in mantle garnets from Arizona could not explain how these minerals might have exsolved stoichiometrically and out of this necessity resorted to an explanation of garnet overgrowing epitaxially attached oxides. Even though epitatctic growth is a rather widespread phenomenon amongst rock-forming minerals if substrate surfaces extend into fluid- or melt-filled space (e.g. Hammer et al., 2010), the percentage of cases where such an orientation relationship develops is lower than in solid state precipitation because heterogeneous nucleation plays a more important role (see also

point 7). During metamorphic recrystallization of a rock free growth surfaces are practically absent and heterogeneous nucleation along irregular grain and phase boundaries is absolutely dominant. Oriented attachment to the growing face of a porphyroblast is hence very rare and not to be expected. Epitaxy is restricted to those few cases with considerable structural similarities (staurolite-kyanite, micas…) or to actual replacement reactions of one mineral by another (topotactic reactions; Dent Glasser et al., 1962; Figlarz et al., 1990). Both criteria do not apply in the case of rutile on/in garnet.

(6) Etch pits and etch channels have their shape and directions controlled by the crystal structure of the mineral. It is unknown, whether garnet can be etched in a way by natural fluids that channels would develop selectively in the 111-directions of the crystal. It is also unknown, but considered highly unlikely by the present authors, that Ti is preferentially transported into such cannels and would precipitate there as rutile. This hypothetical scenario would also involve filling of the remaining void space between the rutile needles by more garnet material during a later stage.

(7) Hwang and co-workers described oriented microcracks in garnet parallel to the {110} cleavage planes of garnet, either caused by overpressured mineral inclusions (Hwang et al. 2001) or by extreme stress in some UHP rocks (Hwang et al., 2007b). These cracks were only partly healed and those around polyphase inclusions (quartz, rutile or brookite, ilmenite, kyanite, staurolite, zircon) contained unoriented TiO_2 nanoparticles that were interpreted as precipitates resulting from the overpressure-induced reaction ilmenite + kyanite = garnet + rutile (GRAIL-geothermobarometer). As these authors did not find a clear crystallographic orientation relationship in a detailed TEM study of oriented rutile needles in UHP garnets with the same SPO characteristics as described here, they ruled out a precipitate origin for this type of rutiles, too, and proposed as one alternative the formation of microcleavage followed by precipitation

of rutile and healing (Hwang et al., 2007a). Rutile needles with no CPO but an SPO determined by the {110} planes of garnet is the main criterion here. It is difficult to apply such a model to our sample because it is not clear how pervasive microcracking in the entire several millimetres thick outer rim of the garnet may have occurred without having an even more intense microcracking in the strongly poikilitic core. There is no TEM evidence for such microcracks either and we have shown that CPO is present, even though it does not reveal itself easily unless a large number of rutile grains is investigated by EBSD. However, in a recent paper on the subject of polymineralic oriented inclusions (kokchetavite, micas, cristobalite and others) in clinopyroxenes from Kokchetav microdiamond-bearing rocks, Hwang et al. (2012) found a number of crystallographic orientation relationships amongst inclusions and host, and argue quite convincingly against an exsolution origin and propose a cleaving-healing event accompanied by oriented deposition. Unless alternative explanations for the observations in Hwang et al. (2012) turn out to be true, like precipitation of a metastable intermediate phase that later decomposed into a polymineralic assemblage, or deposition from melt inclusions, this may represent a well-illustrated example of epitaxial growth in cracks, demonstrating that SPO and CPO can develop in such a situation.

(8) Dissolution-precipitation is the main recrystallization process in metasomatism and also in metamorphism as long as a fluid phase is present. An interesting variety of this process is dissolution of a solid solution mineral accompanied by reprecipitation of the same mineral, often in structural continuity but with different composition. This can be accompanied by precipitation of components dissolved in the mother as separate phases in the daughter crystal. Regional-scale albitization of feldspathic rocks with co-precipitation of nanometer-sized Fe-hydroxides - often in voids generated by the replacement process – serves as an example (Engvik et al., 2008). From a large

number of hydrothermal experiments by Harlov and co-workers some also produced co-precipitates, and in the case of F-apatite treated with sulphuric acid solution even oriented precipitates of monazite were observed in the recrystallized apatite behind the reaction front (Harlov et al., 2005). Natural examples of acicular inclusions of monazite oriented parallel to the c-axis of apatite are known from pegmatites (Amli, 1875) and muscovite schists (Pan et al., 1993). Due to various textural criteria they were interpreted as precipitates and – due to the obvious non-stoichiometry of an exsolution process – some metasomatic influence or "non-stoichiometry" of the original apatite composition was inferred. It is not known whether in any of these cases, including Harlov (2005), a CPO relationship goes along with the observed SPO. If a replacement reaction is dissolution-controlled, interface-coulped dissolution-precipitation results in a volume-by-volume replacement (pseudomorphs), and crystallographic similarities between educt and (polyphase) products may result in a certain degree of crystallographic orientation relationship (Putnis, 2009). Contrary to solid state precipitation, however, such orientation relationships are significantly less common compared to solid state precipitation. Interface energy minimization due to crystallographic similarities is much less important in this case because nucleation is heterogeneous (at the reaction front), so it can be expected that strict orientation relationships are much less common than in the case of homogenously nucleating precipitates. The main additional feature often observed in situations of dissolution-precipitation growth is voids in the replacing material – particularly, but not only, in experimental samples (e.g. Putnis & Austrheim, 2010). These voids provide the necessary fluid pathways towards the replacement front, but they may be just a transient feature that gets eradicated during subsequent annealing in natural rocks. Another rather common feature is cracks, which again are mainly known from dissolution-precipitation experiments and could also be a transient phenomenon that

may or may not be preserved in natural samples. Dissolution-precipitation is a metasomatic process that affects rocks pervasively, but is also the most important mechanism responsible for the recrystallization of metamorphic rocks from low grades to the amphibolite or eclogites facies. There is, however, little evidence in metamorphic rocks that micas or garnets get dissolved along replacement fronts with a new mica or garnet of slightly different composition precipitating behind that front. Garnets with a clear prograde growth zoning in particular are not subject to such processes. If alteration and change of compositions by fluids occurs in a garnet, it usually follows some microcracks or subgrain boundaries into the crystal and causes a compositional alteration of garnet (e.g. Whitney, 1996; Hwang et al., 2012). The altered zones are quite irregular in shape. If the clear rim of garnet 2R5 had formed in this way, the replacement had had to be very regular from all sides, and the compositional zoning in this rim area would have to be an even later phenomenon because dissolution-precipitation should result in a constant chemical composition of the new garnet.

(9) Perchuk (2008) observed oriented rutile needles in the cores of garnets from Kockchetav. Some parts of the inclusion areas were also affected by melt-inclusions. The evidence of polymineralic acicular inclusions that contained sodic and potassic micas in addition to rutile was then interpreted to indicate formation of these inclusions by interaction of garnet with melt. The presence of the large potassium ion in particular is hard to explain by exsolution from even a UHP garnet. On the other hand micas and rutile do not make up a realistic melt composition, and as we have observed no melt droplets in our garnets, or micas as part of the needle substance, we discard this mechanism for sample 2R5. Nevertheless fluid/melt-infiltration is considered also by Hwang et al. (2010) as the cause of oriented ilmenite, spinel,

magnetite, amphibole and garnet inclusions in clinopyroxene from the Sulu UHP terrane.

In summary, and according to our opinion, solid state precipitation seems to be the most likely mechanism of formation. It explains the morphology of the rutile needles, their very regular distribution throughout the garnet rim and the observed SPO and CPO relationships. It is consistent with the garnet zoning pattern and the absence of pores or cracks as well as chemical alteration zones in garnet. It does, however, not at once explain the chemical side of the process because the classical view of exsolution/precipitation considers the host crystal to be a closed system and the process hence to be isochemical.

Open system precipitation.

Ti gets incorporated in many silicates by certain coupled substitutions – those for garnet are listed in Table 3 – but none of the theoretical endmembers are stable under regional metamorphic P-T conditions. Hence Ti cannot exsolve as such an endmember but has to exsolve in the form of other stable Ti-minerals, mainly rutile and ilmenite. This is possible only if the original garnet had a very exotic composition and/or additional phases are involved in the precipitation reaction. Hence all prior efforts to explain elongate rutile with SPO in garnet as solid-state precipitates were based on either a postulated extraordinary, unproven starting composition of garnet (e.g. Zhang et al., 2003), including a high amount of hydrogen (Roden et al., 2006) or tetrahedrally coordinated Ti (van Roermund et al., 2000; Ye et al. (2000)) for which there is no experimental evidence at temperatures below 1200°C (Huggins, 1977; Schwartz et al., 1980; Hermann et al., 2005; Berry et al., 2007, Kawasaki & Motoyoshi, 2007), or on additional minerals present in the garnet, either as educts for a precipitation reaction (Zhang et al., 2003) or as products (co-precipitates). Such an explanation may bear

out in the case of ilmenite co-precipitating with pyroxenes from a formerly majoritic garnet (van Roermund et al., 2000), but no realistic scenario has yet been devised for rutile precipitates, not to speak of rutile precipitating without another co-precipitate.

Hence a more realistic answer may lie in the direction of open-system behaviour, and as we have ruled out mechanisms (2) to (9) above as less probable or irrelevant, the open system is the garnet crystal exchanging material with the intergranular pore space mainly by solid state diffusion – a mechanism we call open system precipitation (OSP). This is not an unrealistic assumption.

From what we know about diffusion at high metamorphic grades (e.g. homogenization of mineral zoning patterns, closure temperatures for ion or isotope exchange etc.) we must expected that minerals behave as (partly) open systems at high temperatures, with the "degree of openness" depending on diffusion constants and boundary conditions only. The host crystal, due to the very fundamental phenomenon of diffusion, is not and never will be an (entirely) closed system. Volume diffusion through a crystal will always transport material into and out of the crystal, and the only question is how effective diffusion can be for the various species available. In order to make clear that this concept goes beyond the standard simplified scenario of a precipitation in a closed (host mineral) system, we use the term "open system precipitation" (OSP), and we use OSP sensu strictu for the hypothetical situation of purely solid state volume diffusion of species, whereas OSP sensu lato would include other diffusion pathways present in natural minerals like dislocations or nanotubes, but we explicitly exclude a thoroughly fluid driven process like dissolution-precipitation from the definition. There aremany ways in which open-system reactions can be written, depending mainly on which species one considers to be most mobile.

In the following we will just give a few examples of possible open system reactions in order to illustrate three different types

We introduce the endmember phase components $M_3(MTi)Si_3O_{12}$ (v2-grt) and $M_3TiAl[AlSi_2]O_{12}$ (v3-grt), which are obtained from an ordinary garnet with composition $M_3Al_2Si_3O_{12}$ by application of the exchange vectors v2 and v3, respectively. Combination of these endmember into a single garnet solid-solution provides potential starting points for the precipitation of rutile from garnet and require different extents of component exchange with the rock matrix.

If these endmember components are combined in the molar proportions 1:3 a reaction may be formulated that where both Al and Si are retained in the garnet solid solution and rutile and metal oxide are produced

$$M_3(MTi)Si_3O_{12} + 3\ M_3TiAl[AlSi_2]O_{12} = 3\ M_3Al_2Si_3O_{12} + 4\ TiO_2 + 4\ MO \qquad (1),$$

v2-grt v3-grt grt ru

The reason why we consider actual oxygen diffusion and loss from the crystal as at least part of the process is explained a bit further below. The alternative, usual way is to formulate reactions with cation diffusion only, in this case we can write an equation for additional Si^{4+} diffusion:

$$M_3(MTi)Si_3O_{12} + 5\ M_3TiAl[AlSi_2]O_{12} + 2\ Si^{4+} = 5\ M_3Al_2Si_3O_{12} + 6\ TiO_2 + 4\ M^{2+} \qquad (1'),$$

v2-grt v3-grt grt ru

In all cases, M represents a divalent cation. Reaction 1' (mobility of Si) is not unlikely because SiO_4-tetrahedra seem to be considerably more mobile and adjustable during topotactic reactions than 6-coordinated small cations (Dent Glasser et al., 1962)

A reasonable alternative high-temperature exchange vector involves vacancies, $\square_{0.5}TiM_{-0.5}Al_{-1}$ **(v5)**, with the pertinent endmember $M_{2,5}TiAlSi_3O_{12}$, or the high-pressure exchange vector $NaTiM_{-1}Al_{-1}$ (v4). See Table 5 for a short summary of reaction equations.

Another interesting alternative is ***precipitation by redox reaction***: The fundamental problem of rutile exsolution is the fact that Ti resides in the octahedral site, and its release

creates vacancies, or rather an over-abundance of Si on the tetrahedral and of M^{2+} cations on the dodecahedral sites. This situation can be overcome to some extent by oxidizing Fe^{2+} to Fe^{3+} and shifting it from the dodecahedral to the octahedral site. As divalent cations can diffuse faster than tri- or tetravalent ones, diffusional supply of divalent cations from the matrix can remedy the situation. The pertinent reaction balance looks appealing with regard to expected diffusion rates:

A precipitation reaction can be formulated as:

$$3\ M^{2+}{}_3TiAl[AlSi_2]O_{12} + 2\ M^{2+}{}_{2,5}TiAlSi_3O_{12} = 4\ M^{2+}{}_3Al_2Si_3O_{12} + 2\ M^{2+}O + 5\ TiO_2, \quad (2)$$

and is valid for an exact ratio of 3:2. If we assume a ratio closer to 1:1, we get:

$$3\ M^{2+}{}_3TiAl[AlSi_2]O_{12} + 3\ M^{2+}{}_{2,5}TiAlSi_3O_{12} = 5\ M^{2+}{}_{3.3}Al_{1.8}[]_{0.2}Si_3O_{12} + 6\ TiO_2; \quad (2a)$$

This equation shows an over-filled dodecahedral site and an under-filled octahedral site. This lattice strain could be compensated by Fe^{2+} from the dodecahedral site oxidizing (releasing an electron) and jumping to the octahedral site. This results in:

$$5\ M^{2+}{}_{3.3}Al_{1.8}[]_{0.2}Si_3O_{12} = 5\ M^{2+}{}_{3.1}Al_{1.8}Fe^{3+}{}_{0.2}Si_3O_{12} + e^-, \quad (4)$$

which is of course an over-filled and overcharged molecule and reacts as:

$$10\ M^{2+}{}_{3.1}Al_{1.8}Fe_{0.2}Si_3O_{12} = 10\ M^{2+}{}_{3.0}Al_{1.8}Fe_{0.2}Si_3O_{12} + M^{2+} + 2\ e^-. \quad (4')$$

This reaction is equivalent to $3\ Fe^{2+} = 2\ Fe^{3+} + Fe^0$ and means that the oxygen balance is maintained at the oxidation site and $Fe^{2+} + 2e^-$ travel elsewhere in a more or less coupled manner (maybe as Fe^0).

The combined reaction equation would be

$$6\ M^{2+}{}_3TiAl[AlSi_2]O_{12} + 6\ M^{2+}{}_{2,5}TiAlSi_3O_{12} =$$

$$10\ M^{2+}{}_{3.0}Al_{1.8}Fe_{0.2}Si_3O_{12} + M^{2+} + 2\ e^- + 12\ TiO_2 \quad (2b)$$

This reaction requires the least amount of diffusing charges per volume (Table 5, last column) of all reactions proposed. Internal redox reactions do exist and have been experimentally investigated in alloys and reported in the material sciences literature by Schmalzried and co-workers under the name “internal solid state reactions” (e.g. Schmalzried and Backhaus-

Ricoult, 1993). Some of their experiments even produced periodical precipitates not dissimilar in spatial distribution to the rutile precipitates presented here. Their reactions involved the diffusion of oxygen through the metal lattice and were fast enough to produce visible results within hours to days at temperatures between ca. 1000 and 1400°C.

Each of the various formulations of open system reactions indicates an alternative mechanism, and all of them will operate to some extent, depending on the relative diffusion rates of the pertinent species – hence all of them will add up to the final result and each of them can be evaluated with regard to its importance.

The reason why we also consider oxygen diffusion possible is that "excess" MO might explain why garnet contains a significant amount of carbonate inclusions, often in polyphase inclusions with an additional H_2O-CO_2 fluid. The high chemical potential of MO built up by the precipitation process would result in diffusional expulsion and a reaction at fluid inclusion sites to form carbonate:

$$MO + CO_2 = MCO_3 \quad (5)$$

Such a scenario of intracrystalline carbonate formation is corroborated by the fact that carbonates only occur in garnet inclusions but not in the rock matrix. The carbonate phases are difficult to analyse due to their small grain size, but a great variety of compositions (magnesite, siderite, ankerite, dolomite, Mg-calcite) was determined at least semiquantitatively. The detailed inclusion study by Perraki et al. (2006) on these and similar garnets has revealed that carbonates occur as apparently monophase inclusions but also as polyphase carbonic inclusions together with CO_2 and/or (disordered) graphite or diamond. Polyphase silicate-carbonate inclusions are also present (Fig 4f).

Relevance of OSP for other rocks

For rocks from the Kimi Complex rutile needles are typical for garnets from metapelitic gneisses and observed only rarely in metabasites. The main reason for this could be the high degree of garnet recrystallisation in the metabasites: Garnet in most of these samples has been strongly deformed and now forms aggregates of small subidiomorphic grains. In addition, the sequestration of jadeite component from omphacite triggers breakdown of garnet to provide its grossular component for plagioclase growth. Hence, old garnet recrystallized to a more ferroan and magnesian, extremely poikilitic variety or even to small euhedral neoblasts in the leucosome. Such garnet can hardly retain rutile needles or is even younger than rutile precipitation. In contrast, garnets in paragneisses have been comparatively Ca-poor from the start. They may be subject to breakdown reactions, as indicated by resorbed grain margins, but their interiors have remained mostly intact and no reduction of grain size by deformation was observed in the majority of the samples.

There is a large number of examples from the literature, particularly from ultrahigh-pressure rocks, where rutile needles with SPO were observed together with pyroxene precipitates in garnet (e.g. Haggerty and Sautter, 1990; Van Roermund and Drury 1998; Van Roermund et al., 2000; Ye et al., 2000; Song et al., 2004; Roden et al., 2006) which could be interpreted quite differently if OSP is considered. Considering pyroxene precipitates separate from rutile results in high recalculated former majorite components in garnet. However, the same phenomenon (rutile and pyroxene co-precipitates) could simply be the result of Ti-unmixing which from a non-majoritic high-temperature garnet which demands co-precipitation of pyroxene to maintain stoichiometry in an OSP reaction like

$$M_3TiAl[AlSi_2]O_{12} + 2\ M_{2,5}TiAlSi_3O_{12} = 2\ M_3Al_2Si_3O_{12} + M_2Si_2O_6 + 2\ TiO_2 \qquad (6)$$

v3-grt v5-grt grt opx ru

Whether a majorite component has been present or not – rutile precipitation indicates that the amounts of majorite component computed from pyroxene precipitates alone, and hence the depths of formation deduced, are severely overestimated, because pyroxene precipitation as a consequence of or together with rutile is not related to and does not require a prior majorite component in garnet (cf. Hwang et al. 2007a).

Reintegration of pyroxene segregated into the matrix (Haggerty and Sautter, 1990; Van Roermund and Drury 1998; Roden et al. 2006) results in even high majorite contents and enormous depths of formation. It should at least be accompanied by a reintegration of segregated rutile as well, but the method is obviously open to considerable error by including genuine matrix phases (rutile or orthopyroxene in this case).

As majorite component has turned out to be a function of temperature, too (see experiments summarized in Draper et al. 2003), a considerable amount of the majorite and titanium substitution may have been caused by extreme temperatures at comparatively moderate mantle depths. If titanium substitutions in garnet were better known and calibrated, the combined majorite and titanium substitutions could be quite useful for geothermobarometry.

Oriented needles of ilmenite in garnet, showing the same SPO as the rutile needles described in this paper, are known from UHP rocks but also from granulite facies terrains (Das et al. 2013, M. Raith, pers. comm.), and can be easily explained by OSP. Magnetite exsolutions in garnet (Brearley & Champness) may well be another case of OSP. We are very certain that a large number of suspect precipitation products that just could not be explained by stoichiometric closed-system precipitation may fall under this heading, and the main challenge for future research will be to properly adjudicate the relative importance of OSP and alternative mechanisms as listed in points (2) to (9) above.

CONCLUSIONS

Crystallographically oriented, mostly acicular rutile grains have formed as precipitates in a pre-existing garnet phase with a high-pressure and/or high-temperature metamorphic history. The precursor Ti-rich garnet rim formed at high temperatures (>800°C) and exsolved rutile during subsequent cooling and annealing throughout the granulite and upper amphibolite facies over a time period of perhaps several tens of millions of years (Krenn et al. 2010). We found clear but complex CPO relationships between the rutile and garnet lattices confirming a precipitate origin. Incompatibility of Ti in the garnet host during cooling causes rutile-precipitation that cannot be mass-balanced under closed system conditions. In contrast, an additional exchange of rapidly diffusing species with the rock matrix or fluid inclusions is required. We refer to this process as "open system precipitation" (OSP), and the appertaining reaction equations can be balanced in several ways. The most reasonable is probably the one that requires minimum diffusional transport of low-charge cations and oxygen (and ideally no oxygen diffusion). The stoichiometries thus obtained need to be consistent with the relative amounts of precipitate phases observed.

All possible OSP reactions run parallel and the fastest process may vary, depending on boundary conditions. Hence a complex overall picture may arise. In the case of sample 2R5 the precipitate distribution is very homogenous throughout the garnet rim. A redox reaction may have been the fastest process, as it requires diffusion of only electrons and divalent cations. Oversaturation and consequent exsolution add thermodynamic and mechanical driving forces (lattice strain due to volume change, precipitation-induced elastic deformation and dislocations (e.g. Doherty, 1983) to diffusion, which is why highly charged cations like Al, Si and Ti are also mobile on a scale of tens to hundreds of micrometers. This effect is very obvious for Ti, which segregates into rutile precipitates, and by the precipitate-free zones along grain boundaries and around some cracks and primary inclusions. The degree of mobility and possible loss (or gain) of Al and Si both remain speculative at this point.

For rocks with a P-T history appropriate to trigger open system precipitation, UHP substitutions, like Ti and P entering garnet in combination with Na (substitution vectors v4 and v6) will be very hard to verify as they would have no chance to be preserved during protracted exhumation through the granulite facies. Ti and P are likely to sequester out forming rutile and apatite, and Na will diffuse out of the garnet structure into the matrix. UHP garnet inclusions in containers that are not only mechanically stable but also have low diffusivities (zircon?) would be necessary to find such evidence. These two substitutions, however, are most likely the result of elevated temperatures at high pressures, and the amounts incorporated in garnet could more strongly depend on T than P (e.g. Brunet, 2006).

It is highly important to consider precipitates of Ti-minerals, for example when trying to estimate conditions of formation of a precursor (possibly majoritic) garnet from pyroxene precipitates, as otherwise the pressure of formation can be considerably overestimated.

This case of open system precipitation presented here demonstrates a general type of behaviour that must be expected in any type of solid solution mineral which has incorporated a type of phase component at some high P-T stage that cannot exsolve isochemically at a later stage. It can be predicted and needs to be checked for in other host minerals. It also means that different (faster) diffusion rates need to be considered for minerals undergoing OSP and that a substantial movement of major chemical components can occur and will have to be considered in geothermobarometry or forward thermodynamic modelling which tries to reconcile measured mineral compositions with predicted ones.

ACKNOWLEDGEMENTS

F. Bernhard, Ch. Bauer, H. Tirk and B. Puhr have assisted in data acquisition. We want to thank S. Chakraborty, E. Essene, W. Griffin, H. Marschall, M. Raith, J. Vry and D. Whitney for information about their observations of oriented rutile needles in a variety of rocks. M. Raith also generously supplied samples from Eastern Ghats, India for comparison. This work

was supported by the Austrian Science Fund (FWF): P16194-N06, P22749-N21 and I471-N19. The latter is part of the international DMG-FWF funded Research Network FOR741 D-A-CH.

REFERENCES

Ague JJ, Eckert JO Jr. (2012) Precipitation of rutile and ilmenite needles in garnet: Implications for extreme metamorphic conditions in the Acadian Orogen, U.S.A. Am Mineral, 79, 840-855.

Amli R (1975) Mineralogy and Rare Earth geochemistry of apatite and xenotime from the Gloserheia Granite <pegmatite, Froland, Southern Norway. Am Mineral, 60, 607-620.

Andreozzi GB, Lucchesi S, Skogby H, Della Giusta A (2001) Compositional dependence of cations distribution in some synthetic $(Mg,Zn)(Al,Fe^{3+})_2O_4$ spinels. Eur J Mineral 13, 391-402.

Armbruster T (1981) On the origin of sagenites: structural coherency of rutile with hematite and spinel structure types. N. Jb. Miner. Mh, 7, 328-334.

Bakun-Czubarow N (2004) Majoritic-like garnets from pyrope lherzolites of Sowie Mountains Block in the Sudetes, Central European Variscides. Abstract 32nd International Geological Congress, Florence, 2004.

Banfield JF, Veblen DR (1991) The structure and origino f Fe-bearing platelets in metamorphic rutile. Am Mineral, 76, 113-127.

Bauer C, Rubatto D, Krenn K, Proyer A, Hoinkes G (2007) A zircon study from the Rhodope Metamorphic Complex, N-Greece: Time record of a multistage evolution, Lithos, 29, 207 – 228.

Berry AJ, Walker AM, Hermann J, O'Neill HSC, Foran GJ (2007) Titanium substitutions mechanisms in forsterite. Chem Geol, 242, 176-186.

Boyanov I, Ruseva M, Dimitrova E (1982) First find of Upper Cretaceous foraminiferes in East Rhodopes, Geologica Balcanica, 12, 20.

Brearley AJ,, Champness PE (1986) Magnetite exsolution in almandine garnet. Min Mag, 50, 621-633.

Brunet F, Bonneau V, Irifune T (2006) Complete solid-solution between $Na_3Al_2(PO_4)_3$ and $Mg_3Al_2(SiO_4)_3$ garnets at high pressure. Am Mineral, 91, 211-215.

Bursill LA, Blanchin MG, Smith DJ (1984) Precipitation phenomena in non-stoichiometric oxides II. {100} Platelet defects in reduced rutiles. Proceedings of the Royal Society of London, A 391, 373-391.

Burton KW (1986) Garnet-quartz intergrowths in graphitic pelites: the role of the fluid phase. Min Mag, 50, 611-620

Dachs, E., 1998. PET; Petrological elementary tools for Mathematica^{TM}. Computers and Geosciences, 24／4, 219–235.

Dachs, E., 2004. PET; Petrological elementary tools for Mathematica^{TM}: an update. Computers and Geosciences, 30／2, 173–182.

Das K, Tomioka N, Ando JI (2013) On oriented ilmenite needles in garnet porphyroblasts from deep crustal granulites: Implications for fluid evolution and cooling history. Lithos 156-159, 230-240.

Dawson JB (1980) Kimberlites and their xenoliths. Springer, New York, 252p.

Dent Glasser LS, Glasser FP, Taylor HFW (1962) Topotactic reactions in inorganic oxy-compounds.

Doherty, R.D., 1983. Diffusive phase transformations in the sold state. In: Physical Metallurgy (eds.Cahn, R.W. and Haasen, P.), p. 933-1030. Elsevier.

Donohue CL, Manning CE, Essene EJ (2001) The temperature and pressure dependence of Zr and Ti substitution in almandine. Abstracts with Programs – Geol Soc Am, 33/6, 251.

Draper DS, Xirouchakis D, and Agee CB (2003) Trace element partitioning between garnet and chondritic melt from 5 to 9 GPa: Implications for the onset of majorite transition in the Martian mantle. Physics of the Earth and Planetary Interiors, 139, 149-169.

Enami M, Bolin C, Yoshida T. Kawabe I (1995) A mechanism for Na incorporation in garnet; an example from garnet in orthogneiss from the Su-Lu Terrane, eastern China. Am Mineral, 80, 5-6: 475-482.

Enea C (2008). The origin of the garnets from the tonalities, Susita Valley. IGC 2008 Abstracts.

Feinberg JM, Wenk HR, Renne PR, Scott GR (2004= Epitaxial relationships of clinopyroxene-hosted magnetite determined using electron backscatter diffraction (EBSD) technique. Am Mineral, 89, 462-466.

Figlarz M, Gerand B, Delahaye-Vidal A, Dumont B, Harb F, Coucou A (1990) Topotaxy, nucleation and growth. Solid State Ionics 43, 143-170.

Force ER, Richards RP, Scott KM, Valentine PC, Fishman NS (1996) Mineral intergrowths replaced by "elbow-twinned" rutile in altered rocks. Can Mineral, 34, 605-614.

Fung AT, Haggerty SE (1995) Petrography and mineral compositions of eclogites from the Koidu Kimberlite Complex, Sierra Leone. Journal of Geophysical Research, 100/B10, 20451-20473.

Gottstein G (2001) Physikalische Grundlagen der Materialkunde. Springer Verlag.

Griffin WL, Jensen BB, and Misra SN (1971) Anomalously elongated rutile in eclogite facies pyroxene and garnet. Norsk Geologisk Tidskrift, 51, 177-185.

Guinel MJF, Norton MG, 2006. The origin of asterism in almandine-pyrope garnets from Idaho. J Mat Sci, 41, 719-725.

Haggerty SE, and Sautter V (1990) Ultradeep (greater than 300 kilometers) ultramafic upper mantle xenoliths. Science, 248, 993-996.

HammerJE, Sharp TG, Wessel P (2010) Heterogenous nucleation and epitaxial crystal growth in magmatic minerals. Geology, 38-4, 367-370.

Hermann J, O'Neill HSC, Berry AJ (2005) Titanium solubility in olivine in the system TiO_2-MgO-SiO_2; no evidence for an ultra-deep origin of Ti-bearing olivine. Contrib Mineral Petrol, 148/6, 746-760.

Huggins FE, Virgo D, Huckenholtz HG (1977) Titanium-containing silicate garnets. I. The distribution of Al, Fe^{3+}, and Ti^{4+} between octahedral and tetrahedral sites. Am Mineral, 62, 475-490.

Hwang SL, Shen P, Yui TF, Chu HT (2001) Defect microstructures of minerals as a potential indicator of extremely rapid and episodic exhumation of ultrahigh-pressure metamorphic rock: implication to continental collision orogens. EPSL 192, 57-63.

Hwang SL, Yui TF, Chu HT, Shen P, Schertl HP, Zhang RY, Liou JG (2007a) On the origin of oriented rutile needles in garnet from UHP eclogitesJ metam Geol, 25, 349-362.

Hwang SL, Shen P, Yui TF, Chu HT (2007b) TiO_2 nanoparticle trails in garnet: implications of inclusion pressure-induced microcracks and spontaneous metamorphic-reaction healing during exhumation. J matam Geol 25, 451-460.

Hwang SL, Yui TF, Chu HT, Shen P, Iizuka Y, Yang HY, Yang J, Xu Z (2008) Hematite and magnetite precipitates in olivine from teh Sulu peridotite: A result of dehydrogenation-oxidation reaction in mantle olivine? Am Mineral, 93, 1051-1060.

Hwang SL, Yui TF, Chu HT, Shen P, Zhang RY, Liou JG (2010) An EAM study of garnet pyroxenite from the Sulu ultrahigh-pressure terrane: formation mechanisms of oriented ilmenite, spinel, magnetite, amphibole and garnet inclusions in clinopyroxene. Contrib Mineral Petrol,

Hwang SL, Yui TF, Chu HT, Shen P, Iizuka Y (2012) A TEM tudy of the oriented orthopyroxene and forsterite inclusions in garnet from Otroy garnet peridotite, WGR, Norway: new insights on crystallographic characteristics and growth energetics of

exsolved pyroxene in majoritic garnet. J metam GeolJohnson WC, White CL, Marth PE et al. (1975) Influence of crystallography on aspects of solid-solid nucleation theory. Metallurgical Transactions, 6A, 911-919.

Kawasaki T, Motoyoshi Y (2007) Solubility of TiO_2 in garnet and orthopyroxene: Ti thermometer for ultrahigh temperature granulites. U.s. Geological Survey and the National Academies, USGS OF-2007-1047, Short Research Paper 038; doi:10.3133/of 2007-1047.srp038.

Kawasaki T, Nakano N, and Osani Y (2011) Osumilite and a spinel+quartz association in garnet-sillimanite gneiss from Rundvagshetta, Lutzow-Holm Complex, East Antarctica. Gondwana Research, 19/2: 430-445.

Konzett J, Proyer A, Frost D, Ulmer P (2007) The Ca-Eskola component in eclogitic clinopyroxene as a function of pressure, temperature and bulk composition – an experimental study to 15 GPa with possible implications for the formation of oriented SiO_2-inclusions in omphacite. Contrib Mineral Petrol, 155, 215-228.

Krenn K, Bauer Ch, Proyer A, Mposkos E, Hoinkes G (2008). Fluid entrapment and re-equilibration during subduction and exhumation: A case study from the high-grade Nestos shear zone, Central Rhodope, Greece, Lithos, 104, 33–53.

Krenn K, Bauer C, Proyer A, Klötzli U, Hoinkes G (2010) Tectonometamorphic evolution of the Rhodope orogen, Tectonics, 29, doi:10.1029/2009TC002513, 2010.

Liati A, Gebauer D, (1999) Constraining the prograde and retrograde P-T-t path of Eocene HP-rocks by SHRIMP dating of different zircon domains: inferred rates of heating, burial, cooling and exhumation for central Rhodope, northern Greece. Contrib Mineral Petrol, 135, 340-354.

Liati, A., (2005) Identification of repeated Alpine (ultra) high-pressure metamorphic events by U-Pb SHRIMP geochronology and REE geochemistry of zircon: the Rhodope zone of Northern Greece. Contrib Mineral Petrol, 150, 608-630.

Litvinovsky BA, Steele IM, Wickham SM (2000) Silicic magma formation in overthickened crust: melting of charnockite and leucogranite at 15, 20 and 25 kbar. J Petrol, 41, 717-737.

Malitesta C, Losito I, Scordari F, Schingaro E (1995) XPS investigation of titanium in melanites from Monte Vulture (Italy). Eur J Mineral, 7, 847-858.

McGetchin T R, Silver LT (1970) Compositional relations in minerals from kimberlite and related rocks in the Moses Rock Dike, San Juan County, Utah. Am Mineral, 55, 1738-1771.

Montel JM, Vielzeuf D (1997) partial melting of metagreywackes II: Compositions of minerals and melts. Contrib Mineral Petrol, 128, 176-196.

Moore RO, Gurney JJ (1985) Pyroxene solid solution in garnets included in diamond. Nature, 318, 553-555.

Mposkos E, Kostopoulos D (2001) Diamond, former coesite and supersilicic garnet in metasedimetary rocks from the Greek Rhodope: a new ultrahigh-pressure metamorphic province established. Earth Planet Sci Lett, 192, 497-506.

Nagel TJ, Schmidt S, Janák M, Froitzheim N, Jahn-Awe S, Georgiev N (2011) The exposed base of a collapsing wedge: The Nestos Shear Zone (Rhodope Metamorphic Province, Greece), Tectonics, 30, TC4009, doi:10.1029/2010TC002815.

Nakano T, Takahara H (1989) Intracrystalline distribution of major elements in zoned garnet from skarn in the Chichibu Mine, central Japan; illustration by color-coded maps. The Can Min, 27/3, 499-507.

O'Brien PJ (1999) Asymmetric zoning profiles in garnet from HP-HT granulite and implications for volume diffusion and grain boundary diffusion. Min Mag, 63/2: 227-238.

Okamoto K, Maruyama S (1998) Multi-anvil re-equilibration experiments of a Dabie Shan ultrahigh-pressure eclogite within the diamond stability field. The Island Arc, 7, 52-69.

Ono S (1998) Stability limits of hydrous minerals in sediment and mid-ocean ridge basalt compositions: Implications for water transport in subduction zones. J Geophys Res, 103 (B8), 18253-18267.

Ono S, Yasuda A (1996) Compositional change of majoritic garnet in a MORB composition from 7 to 17 GPa and 1400 to 1600°C. Phys Earth Planet Int, 96, 171-179.

Pan Y, Fleet ME, Macrae ND (1993) Oriented monazite inclusions in apatite porphyroblasts from the Hemlo gold deposit, Ontario, Canada. Min Mag, 57, 697-707.

Parker KA, Stowell HH, Gatewood M (2010) Geochronology and mid- to lower crustal partial melting in a Creatceous magmatic arc, Fjordland, New Zealand. Abstracts with Programs – Geol Soc Am, 42, 5.

Perchuk A (2008) Unusual inclusions in ganet from the diamond-bearing gneiss of the Erzgebirge, Germany. Geochem Int, 46, 296-303.

Perraki M, Proyer A, Mposkos E, Kaindl R, Hoinkes G (2006) Raman micro-spectroscopy on diamond, graphite and other carbon polymorphs from the ultrahigh-pressure metamorphic Kimi Complex of the Rhodope Metamorphic Province, NE Greece. Earth Planet Sci Lett, 241, 672-685.

Proyer A, Krenn K, Hoinkes G (2009) Oriented precipitates of quartz and amphibole in clinopyroxene of metabasites from the Greek Rhodope: a product of open system precipitation during eclogite–granulite–amphibolite transition. J metam Geol 27, 639-654.

Powell R, Holland TJB (1994) Optimal geothermometry and geobarometry. *Am Min* 79, 120-133

Putnis A (2009) Mineral replacement reactions. MSA Rev. Mineral Geochem 70, 87-124.

Putnis A, Austrheim H (2010) Fluid-induced processes: metasomatism and metamorphism. Geofluids, 10, 254-269.

Ricou LE, Burg JP, Godfriaux I, Ivanov Z (1998) Rhodope and Vardar: the metamorphic olistostromic paired belts related to the Cretaceous subduction under Europe. Geodinamica Acta, 11 (6), 285-309.

Ringwood AE, Lovering JF (1970) Significance of pyroxene-ilmenite intergrowth among kimberlite xenoliths. Earth Planet Sci Lett, 7, 371-375.

Ringwood AE, Major A (1971) Synthesis of majorite and other high pressure garnets and perovskites. Earth Planet Sci Lett, 12, 411-418.

Roden MF, Patino-Douce AE, Jagoutz E, Laz´ko EE (2006) High pressure petrogenesis of Mg-rich garnet pyroxenites from Mir kimberlite, Russia. Lithos, 90, 77-91.

Schmalzried H, Backhaus-Ricoult M (1993) Internal solid state rections. Progr Solid State Chem, 22, 1-57.

Schmidt MW, Poli S (1998) Experimentally based water budgets for dehydrating slabs and consequences for arc magma generation. Earth Planet Sci Lett, 163, 361-379.

Schmidt S, Nagel TJ, Froitzheim N, 2010. A new occurrence of microdiamond-bearing metamorphic rocks, SW Rhodopes, Greece. Eur J Mineral, 22, 189-198.

Snoyenbos DR, Williams ML, Hanmer S (1995) Archean high-pressure metamorphism in the western Canadian Shield. Eur J Mineral, 7/6, 1251-1272.

Schwartz KB (1977) Mössbauer spectroscopy and crystal chemistry of natural Fe-Ti garnets. M.Sc. Thesis, Massachussets Institute of Technology, U.S.A.

Shau YH, Yang HY, Paecor DR (1991) Oriented titanite and rutile inclusions in sagenitic biotite. Am Min, 76, 1205-1217.

Sobolev NV, Lavrent´yev YG (1971) Isomorphic sodium admixture in garnets formed at high pressures. Contrib Mineral Petrol, 31, 1-12.

Song S, Zhang L, Niu Y (2004) Ultra-deep origin of garnet peridotite from the North Quaidam ultrahigh-pressure belt, Northern Tibetan Plateau, NW China. Am Mineral, 89, 1330-1336.

Stachel T, Brey GP, Harris JW (2000) Kankan diamonds (Guinea) I: from the lithosphere down to the transition zone. Contrib Mineral Petrol, 140, 1-15.

Tappert R, Stachel T, Harris JW, Muehlenbachs K, Ludwig T, Brey GP (2005) Diamonds from Jagersfontein (South Africa) messengers from the sub-lithospheric mantle. Contrib Mineral Petrol, 150, 505-522.

Tropper P, Konzett J, Finger F (2005) Experimental constraints on the formation of high-P/high-T granulites in the southern Bohemian Massif. Eur J Mineral, 17, 343-356.

Van Roermund HLM, Drury MR (1998) Ultra-high pressure (P < 6 GPa) garnet peridotites in Western Norway: exhumation of mantle rocks from > 185 km depth. Terra Nova, 10, 295-301.

Van Roermund HLM, Drury MR, Barnhoorn A, De Ronde A (2000) Non-silicate inclusions in garnet from an ultra-deep orogenic peridotite. Geological J, 35, 209-229.

Vrana S (1989) Perpotassic granulites from southern Bohemia. Contrib Mineral Petrol, 103, 510-522.

Wang L, Essene EJ, Zhang Y (1999) Mineral inclusions in pyrope crystals from Garnet Ridge, Arizona, USA: implications for processes in the upper mantle. Contrib Mineral Petrol, 135, 164-178.

Wark DA, Watson EB (2006) TitaniQ: a titanium-in-quartz geothermometer. Contrib Mineral Petrol, 152, 743-754.

Whitney DL (1992) High-pressure metamorphism in the Western Cordillera of North America: an example from the Skagit Gneiss, North Cascades. J metam Geol, 10, 71-85.

Whitney DL (1996) Garnets as open systems during regional metamorphism. Geology 24, 147-150.

Whitney DL, Sidman DJ, Goergen ET, Davis PB (2004) Microstructures and metamorphic crystallization. Abstr. Progr. Geol Soc Am 36, 201.

Yang J, Liu L (2004) Coupled isomorphic substitution and exsolution of pyroxene, rutile, apatite and quartz in supersilicic garnet. Chin Sci Bull, 49/1, 70-76.

Yasuda A, Fujii T (1994) Melting phase relations of an anhydrous mid-ocean ridge basalt from 3 to 20 GPa: Implications for the behaviour of subducted oceanic crust in the mantle. J Geophys Res, 99(B5), 9401-9414.

Ye K, Cong B, Ye D (2000) The possible subduction of continental material to depths grater than 200 km. Nature, 407, 734-736.

Zhang JF, Xu HW, Liu Q, Green HW, Dobrzhinetskaya LF (2011) Pyroxene exsolution topotaxy in majoritic garnet from 250 to 300 km depth. J matam Geol 29, 741-751.

Zhang RY, Liou JG. (1998) Crustal-derived ultramafic-mafic complex in the Dabie-Sulu UHP terrane, China; petrochemistry and its implication. Abstracts with Programs – Geol Soc Am, 30/7, p230.

Zhang RY, Zhai SM, Fei YW, Liou JG. (2003) Titanium solubility in coexisting garnet and clinopyroxene at very high pressure: the significance of exsolved rutile in garnet. Earth Planet Sci Lett, 216, 591-601.

Figure captions

Figure 3a: photomicrograph of garnet 2R5, showing a core rich in primary inclusions and a very inclusion-poor, clear rim, from Krenn *et al.*, 2008.

Figure 3b: photomicrograph of a detail from the clear rim, showing precipitates of rutile with three shape preferred orientations.

Figure 3c: Composition profile of garnet 2R5 from rim to rim with major and trace elements as a.p.f.u. Profile length is 26.4 mm. The 2σ uncertainty for each minor element is indicated by an I-bar. Vanadium was consistently low and is not shown.

Figure 4: Upper hemisphere equal angle projections of EBSD data from rutile inclusions and garnet host. a) Density Plot of Rt [001] calculated by harmonic series expansion with a series rank of 16 and a Gaussian Half-Width of 5°. 15 levels have been plotted with a linear colour scheme from light grey (min = 1) via yellow to red (max = 6.728). Additionally the single Rt [001] datapoints (black dots), as well as the orientations of Grt <111>, Grt <110> and Grt <100> directions of the host grain (open squares) are shown; b) Orientations of Grt <111>, Grt <110> and Grt <100> directions of the host grain. c) Rt [001] directions as single data points with Rt grains constituting a cone around one Grt[111] coloured by a rainbow colour scheme; d) poles to Rt {101} planes, e) Rt<110> directions and f) Rt <100> directions with the same colour coding as Fig 4c)

Figure 5: Rutile grains R7 (a-c), R164 (d-f) and R132 (g-i) selected for FIB-TEM, in transmitted light (a, d, g) and SE-images of the thin section (b, e, h) as well as SE-images of

the FIB cut foils (c, f, i); Arrows and lines labelled A-A', B-B' and C-C' give the positions of the foil cuts; the red square in Fig. 5c) marks the position of the rutile grain R7, which is not visible in the SE image; Fig 5 j) shows the Rt [001] orientations of the selected rutile grains with respect to the density plot of all Rt [001] orientations and the Grt <100>, Grt <110> and Grt <111> directions given as upper hemisphere equal angle projection (contoured as Fig. 4a).

Figure 6: a) Rutile grains 132-1 and 132-2 viewed in STEM mode; b) bright field TEM image of 132-2 and c) close-up of the flat tip (circled) of 132-2; d) HRTEM mode imaging of the interface at the tip, with inset of diffraction pattern obtained from garnet and rutile viewed along a common zone axis; e) grain 132-1 with a smooth, featureless garnet-rutile interface.

Figure 7: a) Rutile 164 with additional Zn-rich spinel (bright) and field of EDX-analysis indicated; b) EDX-spectrum of spinel; c) diffraction pattern of spinel.

Figure 8: a, b) Tip of rutile R164 in bright field imaging at different magnifications; c, d) HRTEM images of two different grain boundaries at the tip as indicated in the insets, and lattice planes of rutile and garnet marked (see main text for further description); e) diffraction pattern obtained at grain boundary position (d), demonstrating minor but significant misfit between garnet and rutile.

Figure 9: a) TEM image of section perpendicular to the rutile long axis of grain R7; b) semiquantitative composition profile across garnet-rutile grain boundary with amorphous zone (boundaries indicated by vertical lines); c) HRTEM image of garnet-rutile grain boundary; d) HRTEM image slightly inside rutile, with irregularities interpreted in combination with the multiplication of reflexes in the $[110]_{ru}$ direction (e) as platelet-type superstructures.

This is a preprint. The final publication is available at Springer via http://dx.doi.org/10.1007/s00410-013-0872-7

Figure 1

Fig. 1a

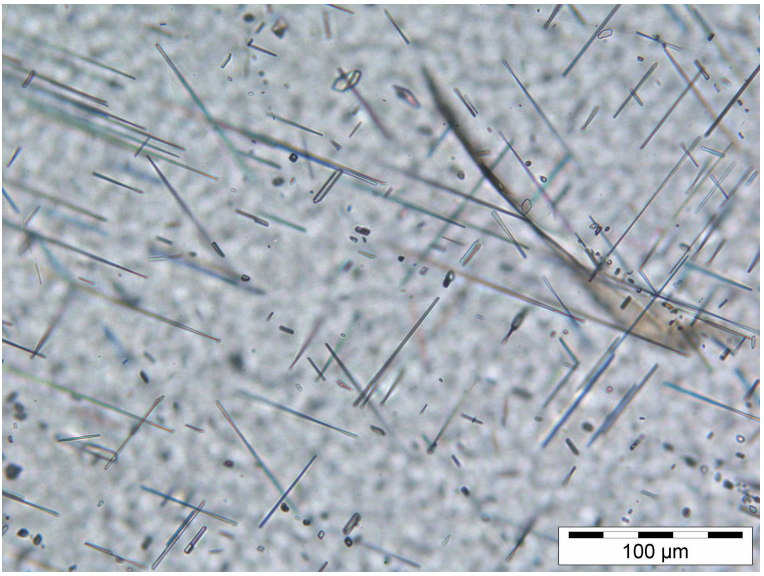

Fig. 1b

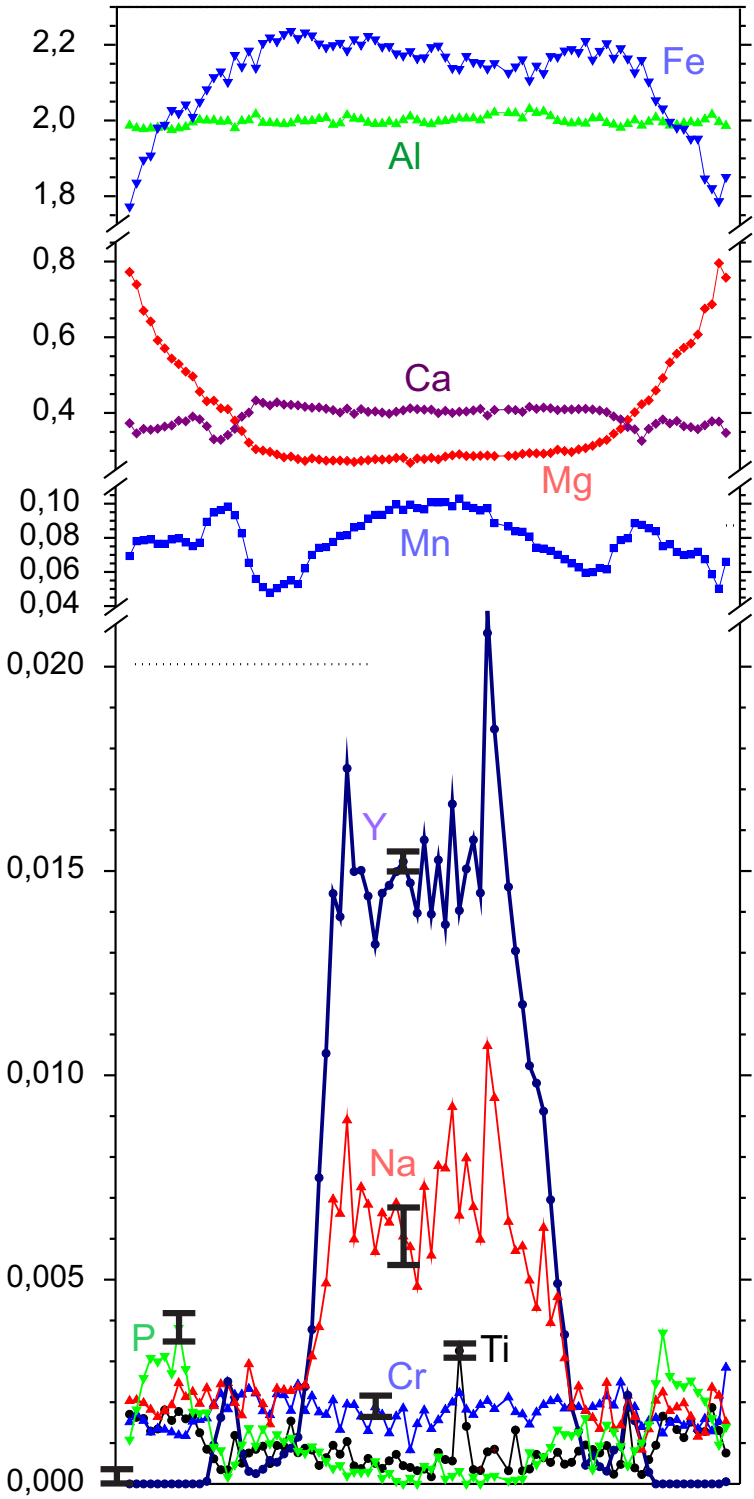

Fig. 1c

Figure 4

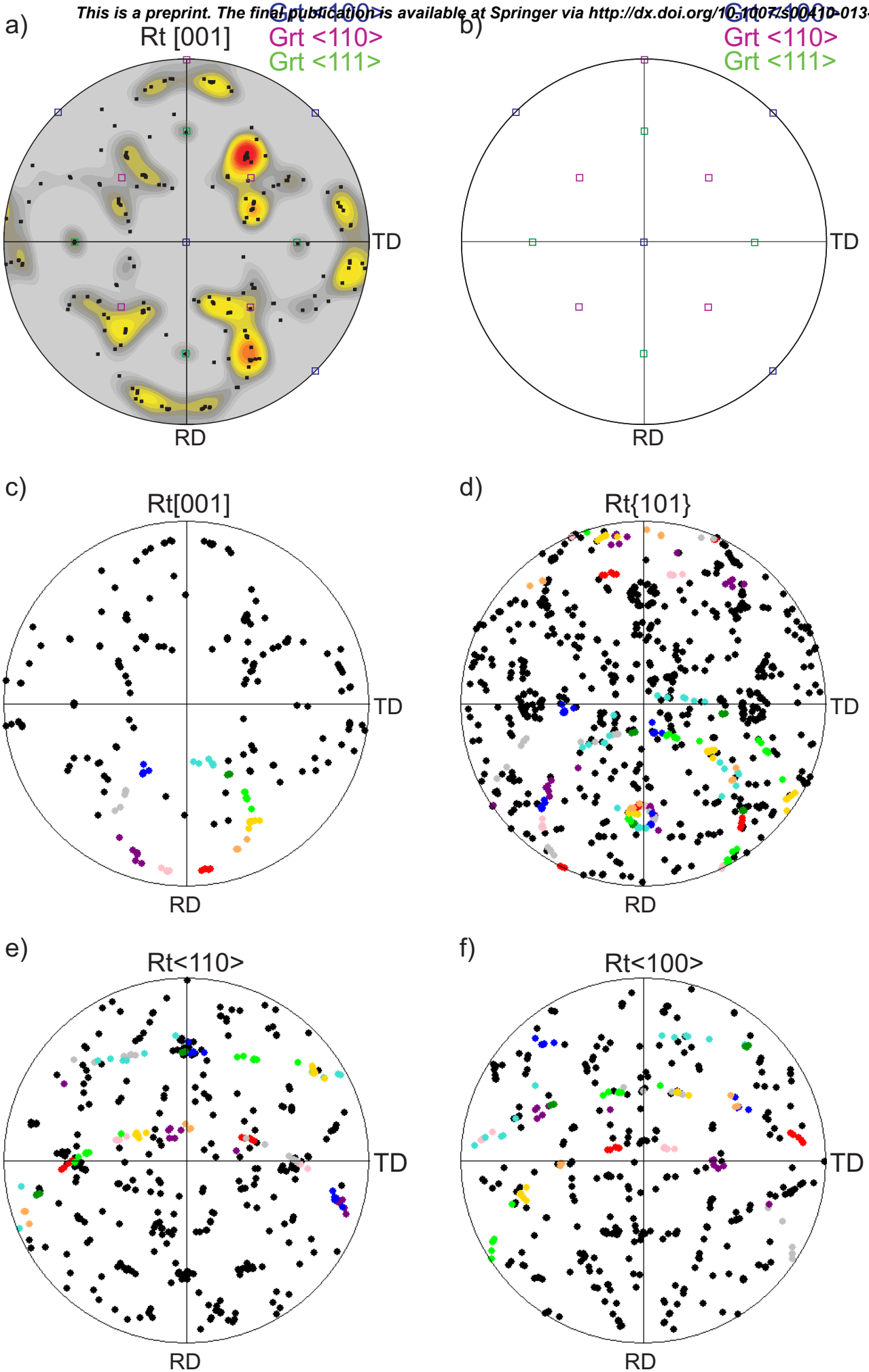

This is a preprint. The final publication is available at Springer via http://dx.doi.org/10.1007/s00410-013-0872-7

Figure 5

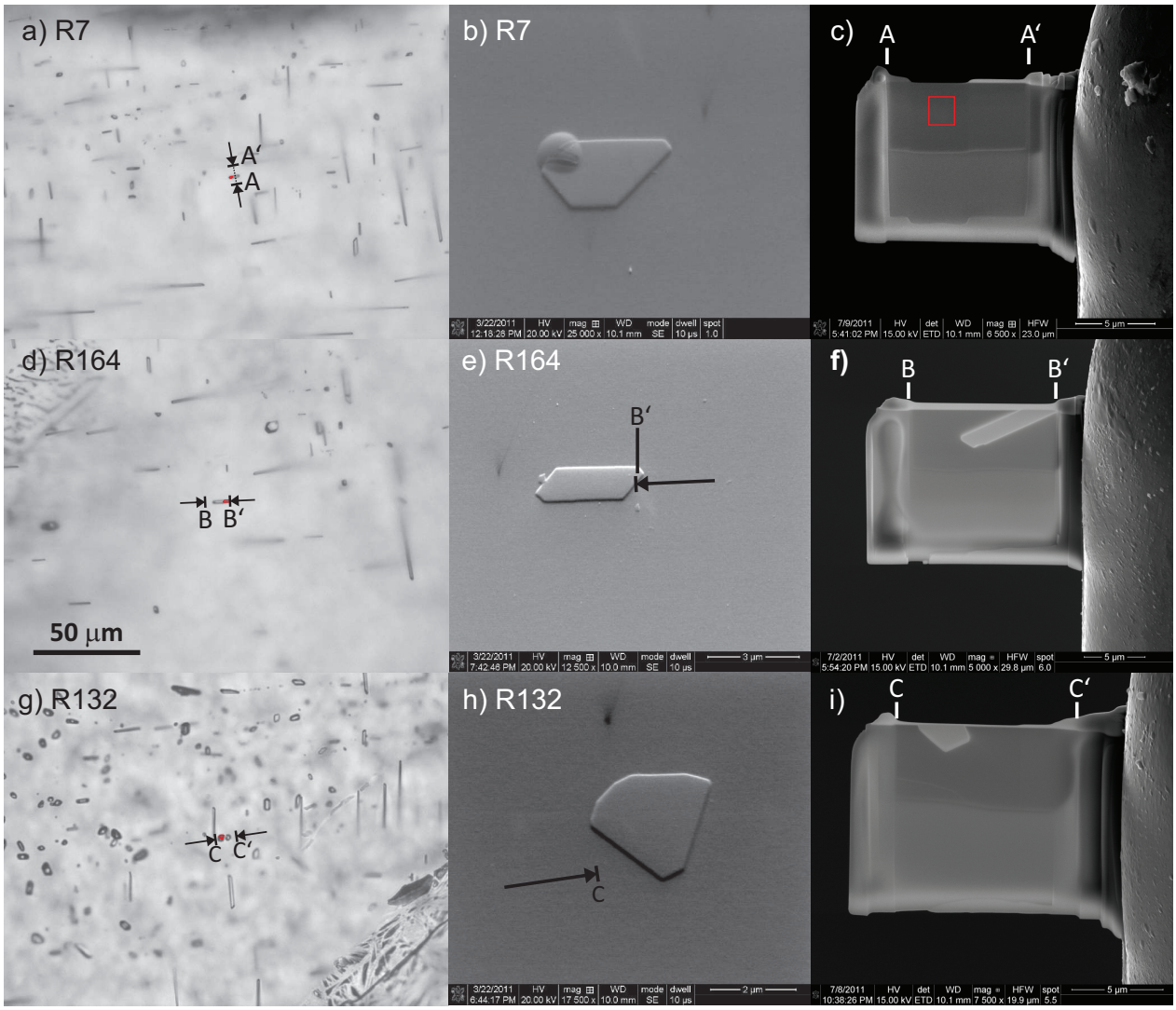

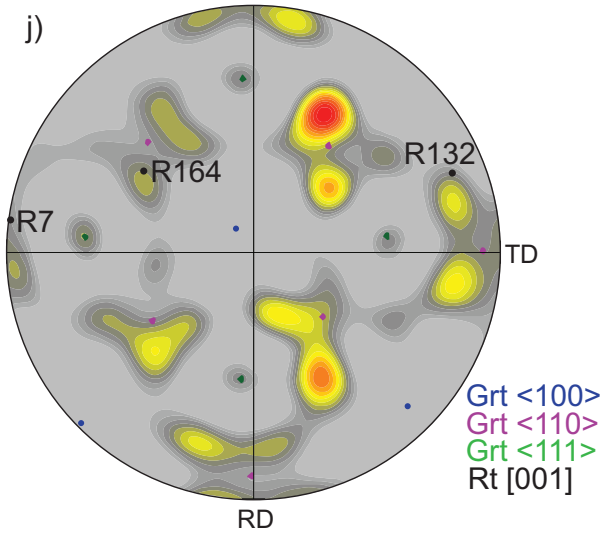

Figure 6

This is a preprint. The final publication is available at Springer via http://dx.doi.org/10.1007/s00410-013-0872-7

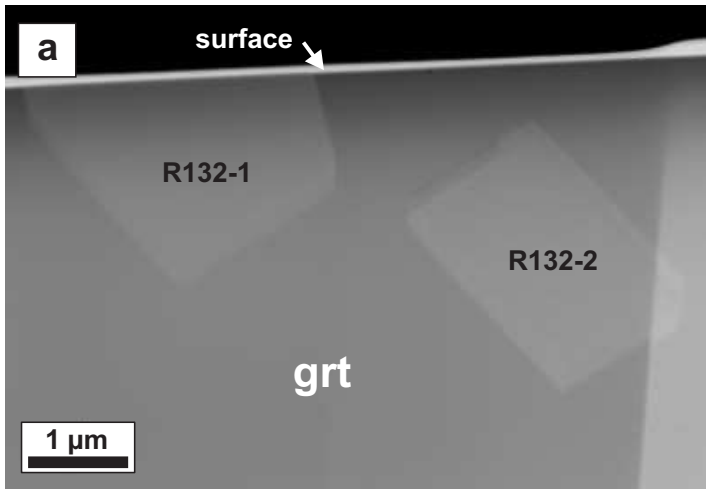

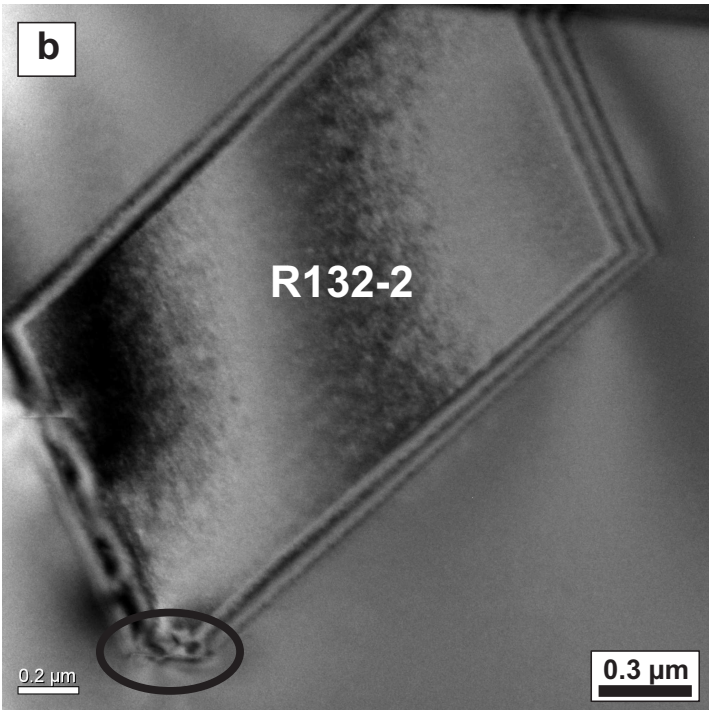

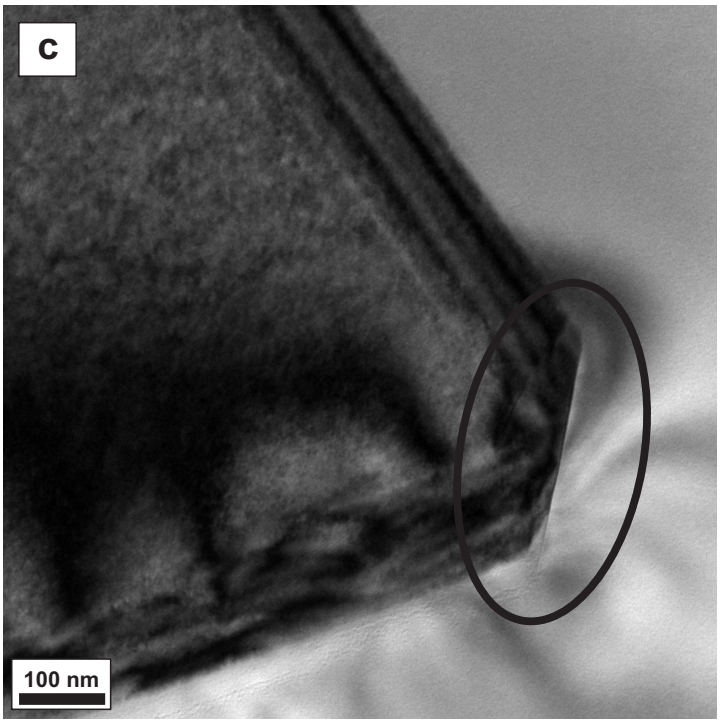

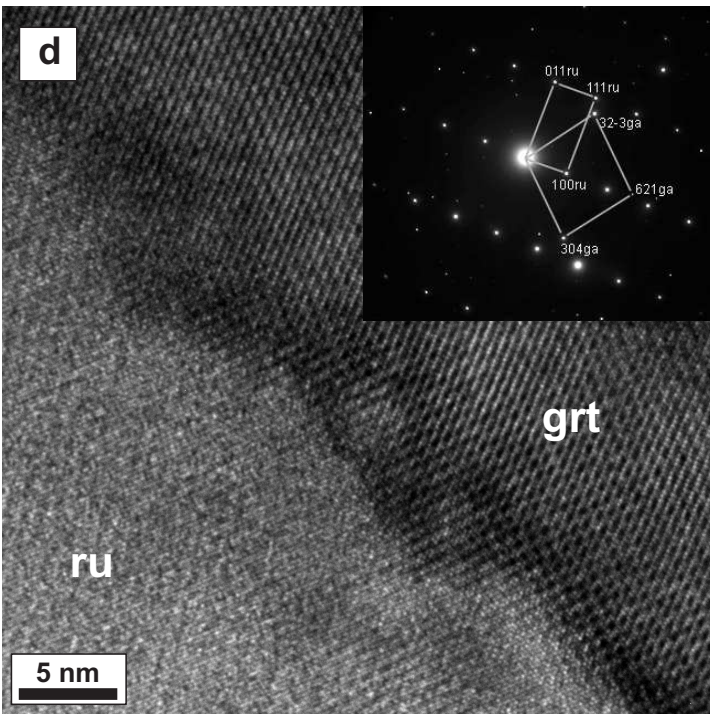

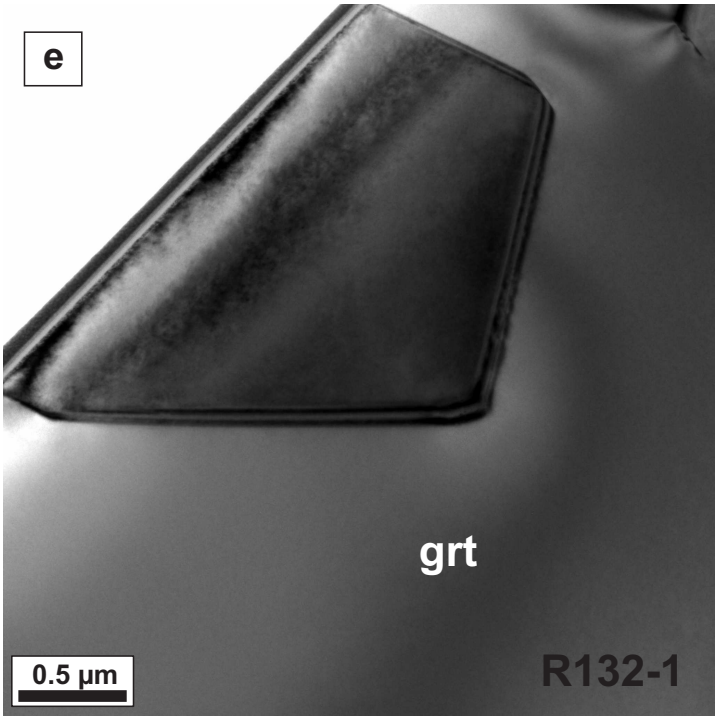

This is a preprint. The final publication is available at Springer via http://dx.doi.org/10.1007/s00410-013-0872-7

Figure 7

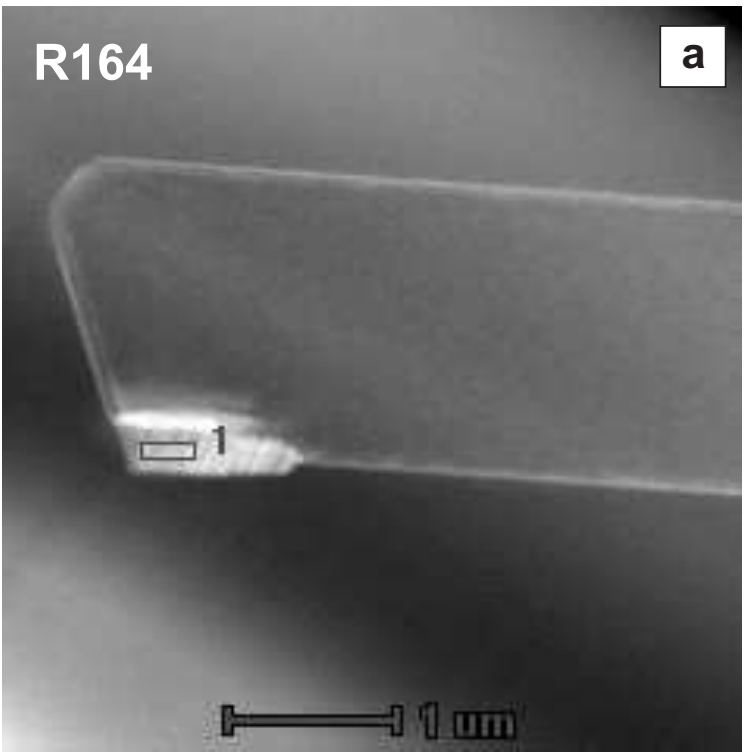

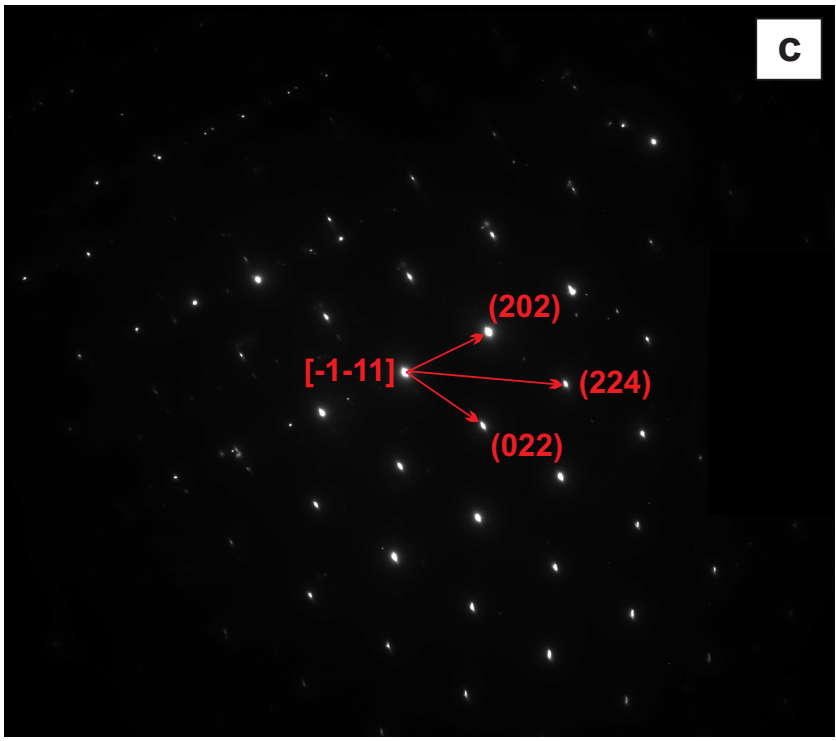

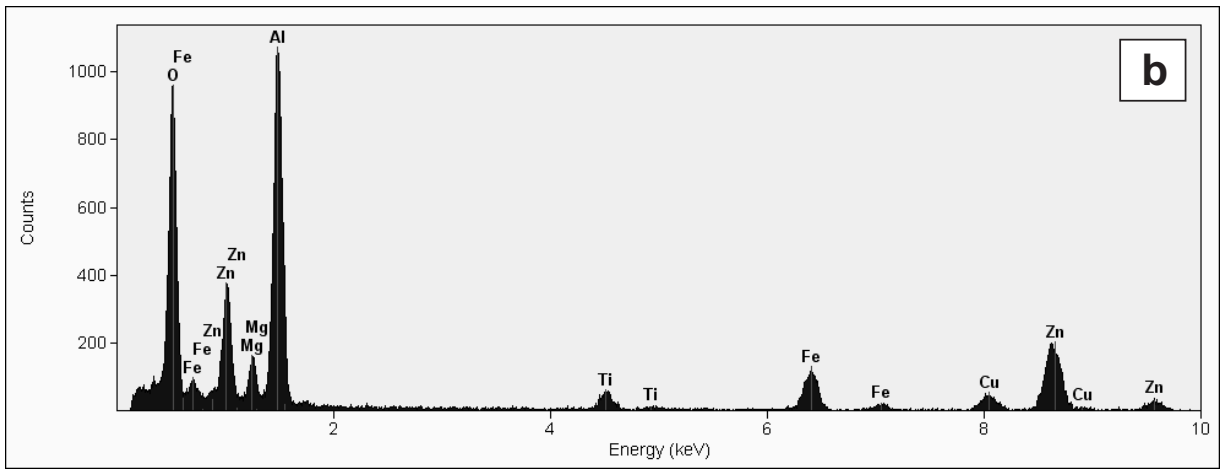

Figure 8

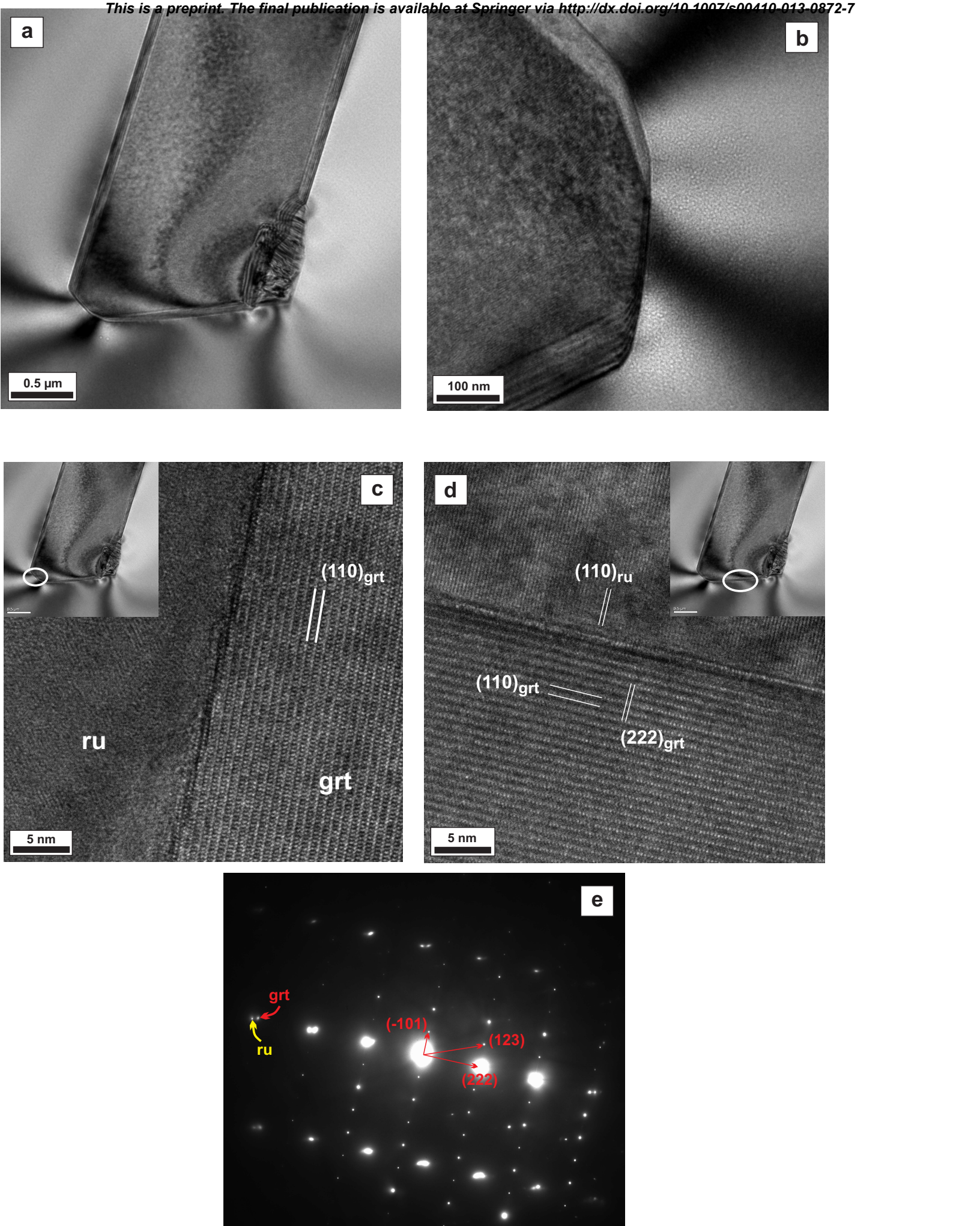

Figure 9

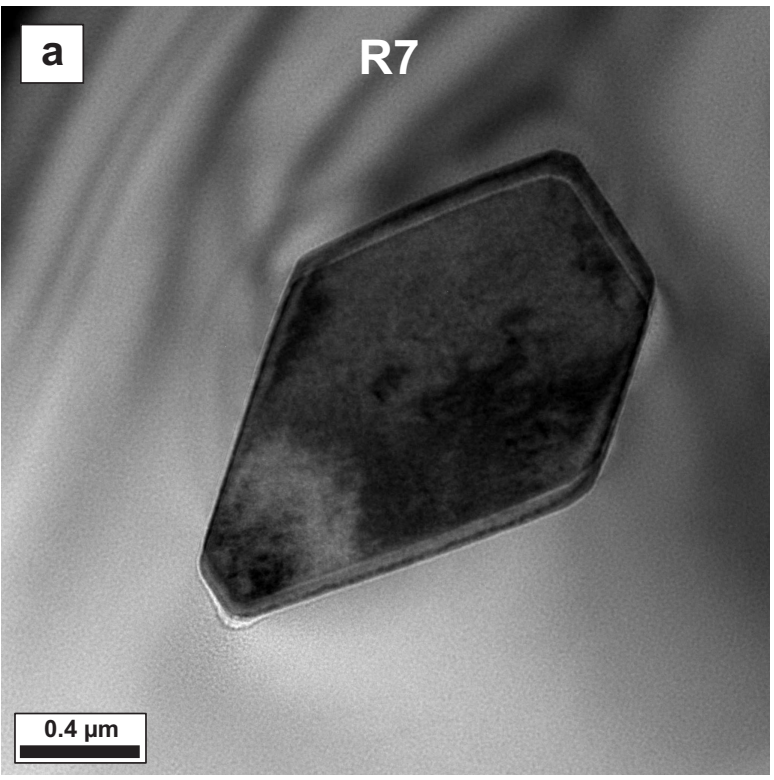

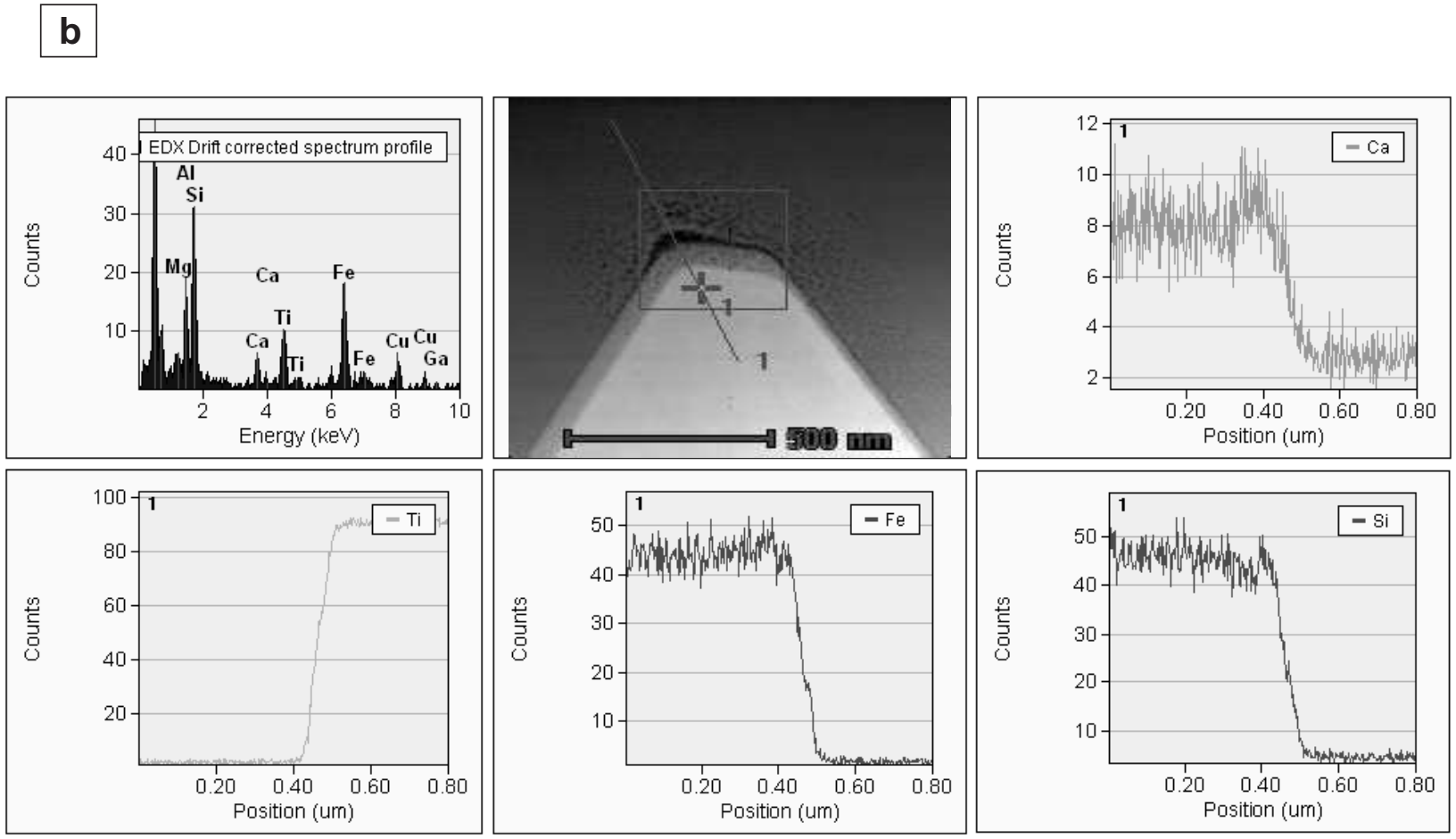

Figure 9 cont.

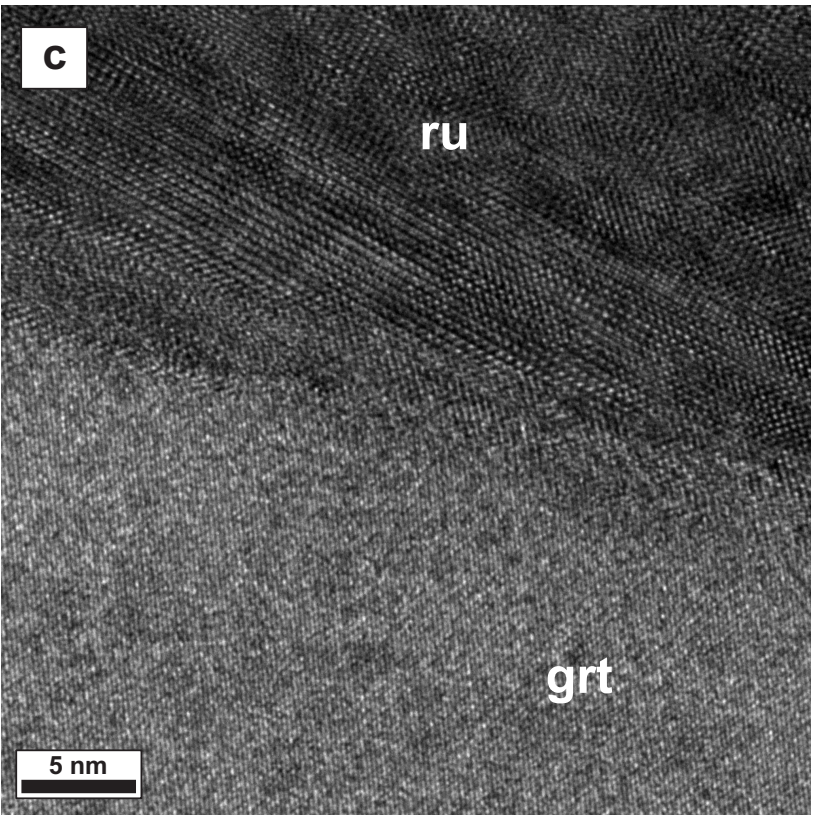

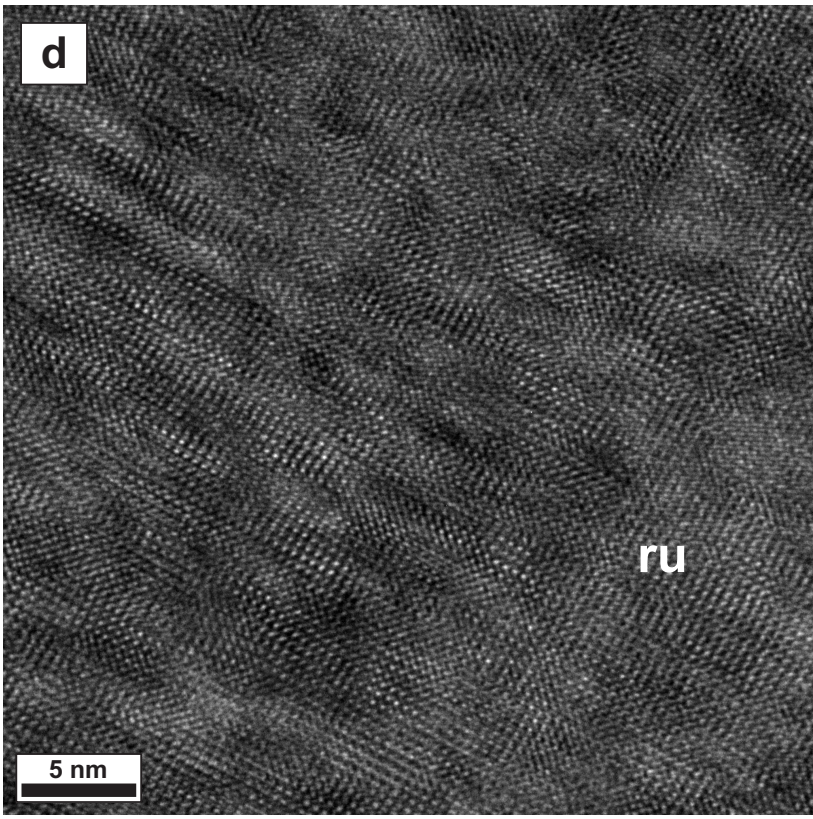

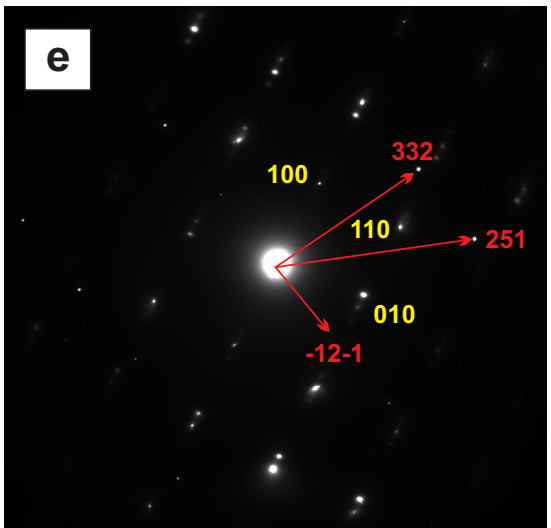

This is a preprint. The final publication is available at Springer via http://dx.doi.org/10.1007/s00410-013-0872-7

Table 1: minute inclusions in the outer ("needle"-) zone of garnet in sample 2R5

site	area (mm^2)	rutile „small"	rutile „big"	rutile + quartz	rutile + kyanite	rt + qtz + ky	quartz	apatite	kyanite	quartz + kyanite	dol / ank	zircon	Fe-Sulfide
0101	0.0331	15											
0102	0.0384	11											
0103	0.0384	19											
0104	0.0380	44			1								
0105	0.0357	20											
0106	0.0384	18											
0107	0.0384	18											
0108	0.0384	17							1				
0109	0.0384	27											
0110	0.0381	26									4		
0301	0.0384	47											
0302	0.0384	53											
0101	0.0384	59	1	2									
0102	0.0384	43		2		1							
0103	0.0381	21			1								
0104	0.0363	33			1								
0105	0.0373	34								1			
0106	0.0374	32		1			1		2				
0107	0.0367	18											
0108	0.0379	19			1				1				
0109	0.0375	24											
0110	0.0375	27											
0111	0.0365	30										1	
0112	0.0384	34											
0113	0.0332	15											
0114	0.0375	16											
0115	0.0331	11											
0201	0.0283	10											
0202	0.0356	21					1						
0203	0.0365	41									2		
0204	0.0384	54		1									
0205	0.0349	27			1						1		
0206	0.0347	24			1						3		(+Dol) 1
0207	0.0375	31			1						4		
0208	0.0365	34									2		
0209	0.0346	26					(?) 1					(+Rt) 1	
0210	0.0361	14	4					(+AlSi) 1				1	
0211	0.0346	11	2				2				(+Rt) 1		
0212	0.0363	19	3				1		1				
0213	0.0361	21											
Total	**1.5464**	**1064**	**10**	**6**	**6**	**1**	**6**	(+AlSi) **1**	**4**	**1**	**13**	**3**	**(+Dol) 1**
per mm^2		688											

rt = rutile, qtz = quartz, ky = kyanite, dol = dolomite, ank = ankerite

This is a preprint. The final publication is available at Springer via http://dx.doi.org/10.1007/s00410-013-0872-7

Table 2

EDX Analyses of areas on TEM-foils in atom wt%, normalized to 100% cations					
	R164 spinel	R7 grt	R7 amorph	R7 ru (rim)	R7 ru (center)
Si		37.54	41.20		
Ti	3.4	0.24	2.92	98.16	99.51
Al	65.9	23.95	26.09		
Fe	7.1	25.69	19.47	1.83	0.48
Mg	7.7	7.41	6.58		
Mn		0.20	0.05		
Zn	15.9				
Ca		4.93	3.60		

Table 3

Possible Ti-substitution mechanisms in garnet

substitution base	substitution vector		(theoretical) endmember	max. Ti-content	valid *P-T* range
andradite $Ca_3Fe^{3+}{}_2Si_3O_{12}$	$^{VI}Ti^{IV}Fe^{3+\,VI}Fe_{-1}{}^{IV}Si_{-1}$	(v1)	$Ca_3Ti_2{}^{4+}(Fe_2{}^{3+}Si)O_{12}$	>25 wt% TiO_2	contact metam.
grossular $Ca_3Al_2Si_3O_{12}$	$Fe^{2+}TiAl_{-2}$	(v2)	morimotoite $Ca_3(Ti^{4+}Fe^{2+})_2Si_3O_{12}$	11.5 wt% TiO_2	contact to regional
pyralspite-garnet $M_3Al_2Si_3O_{12}$	$Ti^{VI}Al^{IV}Al^{VI}{}_{-1}Si^{IV}{}_{-1}$	(v3)	$M_3(Ti^{4+}Al)(AlSi_2)O_{12}$	2.5 wt% TiO_2 (L)	regional metam.
$M_3Al_2Si_3O_{12}$	$NaTiM^{2+}{}_{-1}Al_{-1}$	(v4)	$M_2Na\,(Ti^{4+}Al)Si_3O_{12}$	~2 wt% TiO_2 (OY)	Ultrahigh *P*
$M_3Al_2Si_3O_{12}$	$\square_{0.5}TiM_{-0.5}Al_{-1}$	(v5)	$M_{2,5}TiAlSi_3O_{12}$	unknown	High *T*?

L: Litvinovski et al., (2000); OY: Ono & Yasuda (1996)

Table 4

Rutile exsolution in garnet: Proposed mechanisms from the literature

equation	requirements	L*	main problem	valid *P-T* range
$M_3(MTi)Si_3O_{12} + CaAl_2SiO_6 + SiO_2 = M_3Al_2Si_3O_{12} + CaMSi_2O_6 + TiO_2$	Coesite inclusions or complete recrystallization	Z	Garnet becomes more majoritic during exsolution	P > 5 GPa
$2\,M_{2,5}TiAlSi_3O_{12} + M_3Al_2(TiSi_2)O_{12} = 2\,M_3Al_2Si_3O_{12} + 2\,MSiO_3 + 3\,TiO_2$**	Exchange vectors $\square^{VIII}{}_{0.5}(Si,Ti)^{VI}M^{VIII}{}_{0.5}Al_{-1}$ and ^{IV}Ti	YL	Ti^{4+} most likely not relevant;	UHP?
$2\,M_3(MTi)Si_3O_{12} + 2\,(M_2H)(TiAl)Si_3O_{12} = M_3Al_2Si_3O_{12} + 9\,MSiO_3 + 4\,TiO_2 + H_2O$ or $2\,(M_2H)(TiAl)Si_3O_{12} + 4\,M_3(TiAl)(HSi_{2.75})O_{12} = 3\,M_3Al_2Si_3O_{12} + 7\,MSiO_3 + 6\,TiO_2 + 3\,H_2O$ ***	$^{VIII}H^{+VI}Ti^{VIII}M^{2+}{}_{-1}{}^{VI}Al_{-1}$ and/or $^{VI}Ti\,^{IV}H^{+VI}Al_{-1}\,^{IV}Si_{-0.5}$ ***	R	Exact mechanism not specified or discussed	mantle *P-T*

* L = literature reference; ** reformulated; ***invented following suggestion by R; R: Roden *et al.* (2006), YL: Yang & Liu (2004), Z: Zhang *et al.* (2003).

Table 5

Opens system precipitation reactions and their properties

#	equation	vectors	pre-served	diffusing species	O/Z*
1	$M_3(MTi)Si_3O_{12} + 3\ M_3TiAl[AlSi_2]O_{12} = 3\ M_3Al_2Si_3O_{12} + 4\ TiO_2 + 4\ MO$	v2, v3	Si, Al	M^{2+}, O^{2-}	none
1’	$M_3(MTi)Si_3O_{12} + 5\ M_3TiAl[AlSi_2]O_{12} + 2\ Si^{4+} = 5\ M_3Al_2Si_3O_{12} + 6\ TiO_2 + 4\ M^{2+}$	v2, v3	vol, Al	Si^{4+}, M^{2+}	9:1
1’’	$3\ M_3(MTi)Si_3O_{12} + 3\ M_3TiAl[AlSi_2]O_{12} + 4\ Al^{3+} = 5\ M_3Al_2Si_3O_{12} + 6\ TiO_2 + 6\ M^{2+}$	v2, v3	vol, Si	Al^{3+}, M^{2+}	6:1
2	$2\ M_{2,5}TiAlSi_3O_{12} + 3\ M_3TiAl[AlSi_2]O_{12} = 4\ M_3Al_2Si_3O_{12} + 2\ MO + 5\ TiO_2$	v5, v3	Si, Al	M^{2+}, O^{2-}	none
2’	$2\ M_{2,5}TiAlSi_3O_{12} + 4\ M_3TiAl[AlSi_2]O_{12} + Si^{4+} = 5\ M_3Al_2Si_3O_{12} + 2\ M^{2+} + 6\ TiO_2$	v5, v3	vol, Al	Si^{4+}, M^{2+}	18:1
2’’	$3\ M_{2,5}TiAlSi_3O_{12} + 3\ M_3TiAl[AlSi_2]O_{12} + Al^{3+} = 5\ M_3Al_2Si_3O_{12} + 1{,}5\ M^{2+} + 6\ TiO_2$	v5, v3	vol, Si	Al^{3+}, M^{2+}	24:1
3	$2\ NaM_2TiAlSi_3O_{12} + 3\ M_3TiAl[AlSi_2]O_{12} = 4\ M_3Al_2Si_3O_{12} + Na_2O + MO + 5\ TiO_2$	v4, v3	Si, Al	M^{2+}, O^{2-}	none
3’	$2\ NaM_2TiAlSi_3O_{12} + 4\ M_3TiAl[AlSi_2]O_{12} + Si^{4+} = 5\ M_3Al_2Si_3O_{12} + 2\ Na^{+} + M^{2+} + 6\ TiO_2$	v4, v3	vol, Al	Si^{4+}, M^{2+}	18:1
3’’	$3\ NaM_2TiAlSi_3O_{12} + 3\ M_3TiAl[AlSi_2]O_{12} + Al^{3+} = 5\ M_3Al_2Si_3O_{12} + 3\ Na^{+} + 6\ TiO_2$	v4, v3	vol, Si	Al^{3+}, M^{2+}	24:1
2b	$6\ M^{2+}{}_3TiAl[AlSi_2]O_{12} + 6\ M^{2+}{}_{2,5}TiAlSi_3O_{12} = 10\ M^{2+}{}_{3.0}Al_{1.8}Fe_{0.2}Si_3O_{12} + M^{2+} + 2\ e^{-} + 12\ TiO_2$	v5, v3	vol, Si, Al	M^{2+}, 2 e^{-}	72:1

vol = volume; * O/Z = number of oxygens in the reacting volume divided by the number of diffusing positive charges.